ผลของวิธีการเตรียมต่อแอกทิวิตีของตัวเร่งปฏิกิริยานิกเกิลบนเส้นใยซิลิกาในการรีฟอร์มด้วยไอน้ำของเอทานอล

นางสาวสารีน่า หมัดหมาน

วิทยานิพนธ์นี้เป็นส่วนหนึ่งของการศึกษาตามหลักสูตรปริญญาวิทยาศาสตรมหาบัณฑิต
สาขาวิชาปิโตรเคมีและวิทยาศาสตร์พอลิเมอร์
คณะวิทยาศาสตร์ จุฬาลงกรณ์มหาวิทยาลัย
ปีการศึกษา 2559
ลิขสิทธิ์ของจุฬาลงกรณ์มหาวิทยาลัย

EFFECTS OF PREPARATION METHODS ON ACTIVITY OF Ni/SiO$_2$ FIBER CATALYSTS IN ET
HANOL STEAM REFORMING

Miss Sareena Mhadmhan

A Thesis Submitted in Partial Fulfillment of the Requirements

for the Degree of Master of Science Program in Petrochemistry and Polymer Science

Faculty of Science

Chulalongkorn University

Academic Year 2016

Thesis Title	EFFECTS OF PREPARATION METHODS ON ACTIVITY OF Ni/SiO$_2$ FIBER CATALYSTS IN ETHANOL STEAM REFORMING
By	Miss Sareena Mhadmhan
Field of Study	Petrochemistry and Polymer Science
Thesis Advisor	Associate Professor Prasert Reubroycharoen, Ph.D.

Accepted by the Faculty of Science, Chulalongkorn University in Partial Fulfillment of the Requirements for the Master's Degree

Dean of the Faculty of Science

(Associate Professor Polkit Sangvanich, Ph.D.)

THESIS COMMITTEE

Chairman

(Assistant Professor Sirithan Jiemsirilers, Ph.D.)

Thesis Advisor

(Associate Professor Prasert Reubroycharoen, Ph.D.)

Examiner

(Associate Professor Napida Hinchiranan, Ph.D.)

External Examiner

(Assistant Professor Chanatip Samart, Ph.D.)

สารีน่า หมัดหมาน : ผลของวิธีการเตรียมต่อแอกทิวิตีของตัวเร่งปฏิกิริยานิกเกิลบนเส้นใยซิลิกาในการรีฟอร์มด้วยไอน้ำของเอทานอล (EFFECTS OF PREPARATION METHODS ON ACTIVITY OF Ni/SiO$_2$ FIBER CATALYSTS IN ETHANOL STEAM REFORMING) อ.ที่ปรึกษาวิทยานิพนธ์หลัก: รศ. ดร. ประเสริฐ เรียบร้อยเจริญ, 64 หน้า.

งานวิจัยนี้ศึกษาผลของวิธีการเตรียมตัวเร่งปฏิกิริยานิกเกิลบนตัวรองรับซิลิกาแบบเส้นใย เพื่อใช้ในการเร่งปฏิกิริยาการรีฟอร์มด้วยไอน้ำของเอทานอลสำหรับการผลิตไฮโดรเจน ตัวรองรับเส้นใยซิลิกาที่ใช้ถูกเตรียมด้วยกระบวนการโซล-เจลร่วมกับเทคนิคอิเล็กโทรสปินนิง ตัวเร่งปฏิกิริยาถูกเตรียมด้วย 3 วิธีการ ได้แก่ วิธีการเปียกชุ่ม (Impregnation: IM), การตกตะกอน (Deposition precipitation: DP) และการดูดซับด้วยแรงไฟฟ้าสถิต (Strong electrostatic adsorption: SEA) ตัวเร่งปฏิกิริยาถูกนำมาทดสอบลักษณะเฉพาะด้วยเทคนิคต่างๆ ดังนี้ BET, H$_2$-TPR, XRD, SEM-EDX, TEM และ TGA จากนั้นถูกนำมาใช้ในการเร่งปฏิกิริยาการรีฟอร์มด้วยไอน้ำของเอทานอล โดยสภาวะที่เหมาะสมในการเร่งปฏิริยา คือ การใช้อัตราส่วนโดยโมลของน้ำต่อเอทานอลเท่ากับ 9 ที่เวลาในการเข้าทำปฏิกิริยาเท่ากับ 18 กรัมของตัวเร่งปฏิกิริยาต่อโมลเอทานอลต่อชั่วโมง ในช่วงอุณหภูมิ 400 ถึง 600 องศาเซลเซียส ผลการทดลองพบว่า วิธีการเตรียมตัวเร่งปฏิกิริยามีผลอย่างมากต่อประสิทธิภาพของตัวเร่งปฏิกิริยานิกเกิลบนตัวรองรับเส้นใยซิลิกา การเตรียมตัวเร่งปฏิกิริยาด้วยการดูดซับด้วยแรงไฟฟ้าสถิตให้อนุภาคนิกเกิลออกไซด์ขนาดเล็ก และมีอันตรกิริยาระหว่างโลหะและตัวรองรับเส้นใยซิลิกาที่แข็งแรง โดยขนาดของนิกเกิลออกไซด์ที่เตรียมด้วยวิธีการต่างๆอยู่ในช่วง 7 ถึง 22 นาโนเมตร ตัวเร่งปฏิกิริยาที่เตรียมด้วยวิธีการดูดซับด้วยแรงไฟฟ้าสถิตให้ประสิทธิภาพในการเร่งปฏิกิริยาสูงที่สุด และลำดับของตัวเร่งปฏิกิริยาที่ให้ค่าร้อยละการเปลี่ยนเอทานอลจากมากไปน้อย คือ Ni/SF-SEA > Ni/SF-DP > Ni/ SF-IM > Ni/SP-IM โดยการให้ประสิทธิภาพของตัวเร่งปฏิกิริยาที่แตกต่างกันเป็นผลมาจากขนาดอนุภาคนิกเกิลและอัตรกิริยาระหว่างนิกเกิลและตัวรองรับเส้นใยซิลิกา

สาขาวิชา   ปิโตรเคมีและวิทยาศาสตร์พอลิเมอร์   ลายมือชื่อนิสิต ....

ปีการศึกษา 2559   ลายมือชื่อ อ.ที่ปรึกษาหลัก ....

5772253323 : MAJOR PETROCHEMISTRY AND POLYMER SCIENCE

KEYWORDS:

SAREENA MHADMHAN: EFFECTS OF PREPARATION METHODS ON ACTIVITY OF Ni/SiO$_2$ FIBER CATALYSTS IN ETHANOL STEAM REFORMING. ADVISOR: ASSOC. PROF. PRASERT REUBROYCHAROEN, Ph.D., 64 pp.

The purpose of this research was to study the effects of preparation methods on Ni/SiO$_2$ fiber catalyst for apply to investigate catalytic activity for hydrogen production in ethanol steam reforming (ESR). The catalysts were prepared by three different methods: impregnation (IM), deposition precipitation (DP) and strong electrostatic adsorption (SEA). Silica fiber (SF) supported nickel catalyst have been synthesized by using a combination of a sol-gel method and electrospinning technique. The prepared catalysts were characterized by BET, H$_2$-TPR, XRD, SEM-EDX, TEM and TGA technique. The catalytic tests were performed at atmospheric pressure by using the steam/ethanol mole ratio of 9 and the space time of 18 $g_{catalyst} \cdot h/mol_{ethanol}$ between 400 and 600°C. According to the results, the preparation method had a strong affect on catalytic performance of Ni/SiO$_2$ fiber catalysts used in the ethanol steam reforming. The fiber catalyst prepared by strong electrostatic adsorption method was smaller NiO particle size and stronger metal-support interaction than deposition precipitation and impregnation methods. The NiO particle size in the nickel supported on silica fiber catalyst ranged from 7 nm to 22 nm. The highest catalytic activity was Ni/SF-SEA and their catalytic activity were ordered by Ni/SF-SEA > Ni/SF-DP > Ni/ SF-IM > Ni/SP-IM. The different catalytic activities were related to the particle size and metal-support interaction.

Field of Study: Petrochemistry and   Student's Signature ....

                      Polymer Science   Advisor's Signature ....

Academic Year: 2016

ACKNOWLEDGEMENTS

CONTENTS

LIST OF TABLES

LIST OF FIGURES

LIST OF ABBREVIATION

Ni	Nickel
SiO_2	Silicon dioxide (silica)
CO	Carbon monoxide
CO_2	Carbon dioxide
CH_4	Methane
C_2H_4	Ethene
C_2H_6	Ethane
C_2H_5OH	Ethanol
C_2H_4O	Acetaldehyde
EtOH	Ethanol
TEOS	Tetraethyl orthosilicate
HCl	Hydrochloric acid
N_2	Nitrogen
H_2	Hydrogen
He	Helium
NH_3	Amonia
wt.%	Weight percent
wt.	Weight
T	Temperature
P	Pressure
C	Degree Celsius
XRD	X-ray Diffraction
TPR	Temperature-programmed reduction
TGA	Thermogavimetric analysis
GC	Gas chromatograph
TCD	Thermal conductivity detector
FID	Flame ionization detector
Atm	Atmospheric pressure
μm	Micron meter

cm^3	Cubic centimeter
ml	Mililiter
min	Minute (s)
g	Gram
et al.	And others
MW	Molecular weight
SEA	Strong electrostatic adsorption
IM	Impregnation
DP	Deposition precipitation

CHAPTER I

INTRODUCTION

1.1. Statement of problem

In the future, hydrogen will become an important source of alternative energy due to environmental aspects [1]. It can be used in the fuel cell which is described as operate the electricity with high efficiency [2]. Hydrogen production for ethanol steam reforming is an interesting process as ethanol is low cost, less in toxicity, and easy to transport and store. This process is achieved by using different catalysts. The catalyst has an important and essential part to get total conversion of ethanol because it increases the rate of reaction. The catalysts used in ethanol steam reforming is classified into two types: nobel metal catalysts (e.g., Rh, Ru, Pt, Pd, and Ir) [3-5] and non-noble metal catalysts (e.g., Ni, Co, Mn, and Cu) [5-10]. Although noble-metal catalysts exhibit high catalytic performance in ethanol steam reforming [11, 12] but they are high cost and low reserve. Thus, the development of a non-noble catalytic system with high catalytic performance is an important thing in the ethanol steam reforming. Among base metals, Ni-based catalysts have been widely used in ESR process due to their superior ability of C–C, C–H, and C–O bond cleavage and comparatively low cost [13-16]. Generally, Ni catalyst impregnation on porous silica was high activity and H_2 selectivity in ethanol steam reforming. However, Ni-based porous catalyst have a strong tendency to form coke when high amount of coke are deposited, that can be block catalyst pore which causes the catalyst deactivation and reactor plugging [15].

Silica fiber can be proven the pore blocked. Nonetheless, silica fiber non-pore and weak metal support interaction properties. It can lead to large particle size and low dispersion of metal. Hence, a continuous effect have been made in order to develop Ni-based fiber catalyst with high activity and resistance to coke deposition with time on steam in ethanol steam reforming. Especially, the catalyst preparation method greatly effects to the performance of catalyst. Ethanol steam reforming catalyst have been prepare by varies method such as impregnation, deposition precipitation strong electrostatic adsorption and polyol method.

Impregnation is a widely used method for catalyst preparation which generally result in large particle size and wide distribution for especially high metal content [16].

Deposition precipitate method can be used to lay a high dispersed of metal on the support. This method is important to control base addition to avoid concentration gradient during precipitation [17].

Strong electrostatic adsorption method is based on electrostatic interaction of opposite charged metal co-ordination complex adsorb in well dispersed monolayer [18]. The surface area can be controlled by the pH, temperature of the solution and aging procedures.

In this work Ni-based fiber catalyst with the same nickel content was synthesized by impregnation, deposition precipitation and strong electrostatic adsorption methods. The effect of preparation methods on the activity of catalyst in ethanol steam reforming will be studied.

1.2. Scope of research

The research procedures were carried out as follows:

1. Literature review
2. Prepare silica fibers by electrospinning technique
3. Prepare Ni supported on silica porous (Ni/SP) and silica fibers (Ni/SF) catalysts by impregnation method
4. Study the effect of reaction condition on ethanol conversion and product distribution in ethanol steam reforming.
5. Analyze the gas and liquid products by gas chromatography with thermal conductivity detector and flame ionization detector (GC-TCD&FID)
6. Prepare silica fibers supported Ni catalysts by using impregnation, deposition precipitation and strong electrostatic adsorption method.
7. Study the effect of preparation methods on the activity of Ni-based silica finer catalysts in ethanol steam reforming.
8. Characterize catalysts as follows:

Nitrogen adsorption isotherm   (BET)

X-ray diffraction (XRD)

Temperature-programmed reduction (H_2-TPR)

Scanning electron microscope (SEM)

Transmission electron microscope (TEM)

Energy dispersive X-ray (EDX)

Thermogravimetric analysis (TGA)

9. Summarize the result and write thesis.

1.3. Objective

To prepare silica fiber (SF) support by the electrospinning technique.

To prepare Ni supported on SF (Ni/SF) catalyst by different methods.

To compare the catalytic activity of Ni/SF prepared by several methods for ethanol steam reforming.

CHAPTER II

THEORY AND LITERATURE REVIEW

2.1. Hydrogen production

Hydrogen production is an increased attention in the search to produce renewable hydrogen safely and cleanly. It can be produced from different sources. Among the renewable sources, ethanol from biomass is very attractive due to high hydrogen content, good availability, low cost, non-toxicity, and easy to storage and handling. Production of renewable hydrogen energy comprises of thermo-chemical: (i.e., pyrolysis, gasification, steam gasification, supercritical water gasification of biomass and steam reforming of bio-fuels), electrochemical, photo-biological and photo-electrochemical methods. Among thermo-chemical technologies, ethanol steam reforming is most widely used to generate hydrogen. Ethanol steam reforming (ESR) is an endothermic reaction and thus it requires heat energy to generate hydrogen (Eq.(1)). The major challenge is to minimize the heat energy. Catalysts play an important role in minimizing the heat energy.

2.2. Ethanol steam reforming (ESR)

The principal reaction of ethanol steam reforming (ESR) reaction is presented in Eq. 1. This reaction is an endothermic reaction which ethanol reacts with water at high temperature and produces hydrogen and CO_2 at a H_2/CO_2 ratio of 3.

$$C_2H_5OH + 3H_2O \longrightarrow 2CO_2 + 6H_2 \tag{1}$$
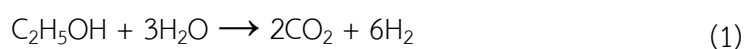
During ESR reaction, there are possible reactions occurring with the principal steam reforming reaction [19]. These reactions are ethanol dehydrogenation (Eq.(2)), ethanol decomposition (Eq.(3)), decarbonylation (Eq.(4)) ethanol dehydration (Eq.(5)), water-gas shift (Eq.(6)), hydrogenatio (Eq.(7,8)), and methane steam reforming (Eq.(9)) as followed Eqs. 1-9.

Ethanol dehydrogenation $C_2H_5OH \longrightarrow C_2H_4O + H_2$ (2)

Ethanol decomposition $C_2H_5OH \longrightarrow CH_4 + CO + H_2$ (3)

Decarbonylation $C_2H_4O \longrightarrow CO + CH_4$ (4)

Ethanol dehydration $C_2H_5OH \longrightarrow C_2H_4 + H_2O$ (5)

Water-gas shift $CO + H_2O \longrightarrow H_2 + CO_2$ (6)

Hydrogenation $CO + 3H_2 \longrightarrow CH_4 + H_2O$ (7)

Hydrogenation $CO_2 + 4H_2 \longrightarrow CH_4 + 2H_2O$ (8)

Methane steam reforming $CH_4 + H_2O \longrightarrow 3H_2 + CO$ (9)
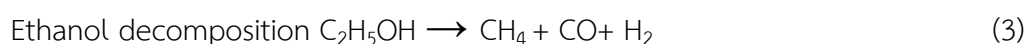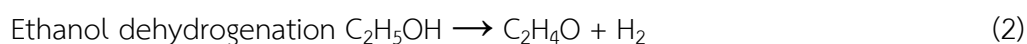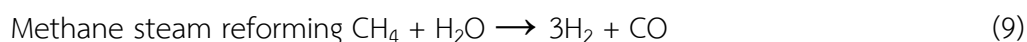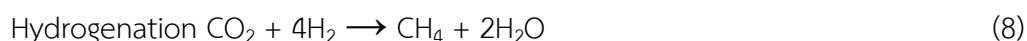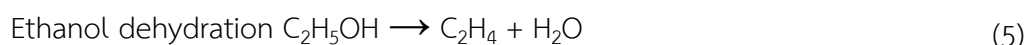
The main of reactions occurs during the steam reforming of ethanol. Both the dehydrogenation to the acetaldehyde and dehydration to ethylene occur depending on the nature of the support. Acidic supports, like alumina, promote ethanol dehydration (Eq.(5)) to produce ethylene, which is a precursor of coke formation [19] while a high surface basicity is favoured dehydrogenation rather than dehydration (Eq.(2)). Acetaldehyde formed undergoes decarbonylation to produce CO and CH_4 (Eq.(4)) and it has a very low coking activity. Furthermore, CO as well as CO_2 on hydrogenation can be converted into CH_4. Carbon monoxide can be produced hydrogen and carbon dioxide via water gas shift reaction (Eq.(6)) whereas CH_4 generates hydrogen through steam reforming (Eq.(9)). Therefore, during ESR along with several other gases such as CO, CH_4, and CO_2 are produced

Moreover, the importance of overall reaction is controlled by operating conditions of the reaction for example temperature, steam/ethanol (S/E) molar ratio, space time and most significantly the selection of catalyst. The effect of operating parameters on distribution of product during ESR was thermodynamically [19] as well as experimentally [15] were reported at several literatures. Its thermodynamics, the reaction occurs at higher temperature range of 300°C and 800°C. The study of ESR over Ni/SiO_2 catalysts at temperature range between 300°C and 700°C by Vicente et al. [20] explained that at higher temperature, ethanol conversion and selectivity of CO, CO_2 and H_2 get increased [20]. At high temperature, reverse water gas shift reaction is responsible reaction lead to low the H_2 yield [21]. Commonly, a steam to ethanol (S/E) molar ratio of 3 is stoichiometrically sufficient for the reaction. However, the excess water favors ethanol decomposition and water gas shift reaction Hacker et al. [22] studied the relation between temperature and water to ethanol feed ratio.

The steam/ethanol molar ratio higher than 4 at reaction temperature range (600-700°C) able to produce more than 4 moles of H_2. Selectivity of H_2 was increased with increasing of S/E molar ratio. Depending on the formulation of catalyst and the reaction operation conditions such as reaction temperature, pressure, steam/ethanol molar ratio and space time, a various intermediates of reaction may be present.

2.3. Catalysts for ethanol steam reforming

The catalysts for ESR reaction was classified in supported noble metals and non-noble metals.

2.3.1. Noble metals-based catalysts

As mentioned before, noble metal catalysts are well-known for their high catalytic activity in any type of reactions involving hydrocarbon activation, especially when the formation of coke by cracking has to be avoided. Noble metal catalysts such as Rh, Pt, Pd and Ru have been reported to be effective catalysts for ESR.

2.3.1.1. Rh-based catalyst

Descorme et al. [23] compared the catalytic activities of Rh/Al_2O_3 versus Ni/Al_2O_3 catalysts for ESR at 600°C. They were found that Rh and Ni catalysts were active and high selective to H_2 production. Their results found 100% conversion of ethanol and 73% hydrogen selectivity over Rh/Al_2O_3 while Ni/Al_2O_3 appeared 76% ethanol conversion. In fact, they had demonstrated that Rh and Ni are active in the ethanol steam reforming [23]. Rh/Y_2O_3 was found to produce the highest rate of H_2 in ESR due to the synergetic effect of electron-accepting Y_2O_3 with electron-donating Rh, whereby the strong oxidizing ability of Y_2O_3 oxidizes the H_2 of ethanol to form H_2 gas and the easy reducibility of Rh reduces the H_2 from water to form H_2 gas [24]. Wang et al. [25] evaluated the performance of Rh catalysts on various supports and found that the order of catalyst activity as follows: Rh/Y_2O_3 > Rh/CeO_2 > Rh/ La_2O_3 > Rh/Al_2O_3. Moreover, among other noble metals, Rh has shown to be more active as it has the highest activity to C-C bond cleavage in ESR [26, 27].

2.3.1.2. Pt-based catalyst

Pt is also a suitable catalyst for both ESR and WGSR. Buitrago et al. [28] has reported that Pt/CeO_2 were important because they have oxygen storage in the Ce_2O structure lead to high catalyst activity [29]. Wang et al. [30] evaluated the activity of Pt, Ir and Co catalysts on Ce_2O support and found that Pt/Ce_2O catalyst is the most active catalyst in term of ethanol conversion [30]. A stronger interaction between Pt oxide nanoparticle and support lead to the high H_2 yield and low coke formation. The order of activity as follows: Pt/CeO_2 > Pt/ZrO_2 > Pt/TiO_2 ~ Pt/C [31]. The ethanol decomposition to CH_4 and CO and ethanol dehydrogenation to CH_3CHO were the primary reactions over Pt-Co, Pt-Ni and Ir catalysts, and they were importantly active and selective for H_2 yield in ESR [32-35]. Pt/CeO_2 catalyst was active and stable at low temperature range of 400-500°C, in comparison to Pt/Al_2O_3 [35]. Increasing of Pt loading enhances the conversion of WGS reaction from CO to CO_2, thus removing CO from the reformate stream. Other noble metals for example Pd, Ir and Ru have been tested in ESR. However, concern level for these noble metals is lower due to poorer catalytic properties than Rh and Pt catalyst.

2.3.2. Non-noble metals-based catalysts

However, the high cost of noble metals is a major limiting factor in their use for hydrogen production via steam reforming. Some selected studies on ethanol steam reforming over non-noble metal catalysts are reported.

2.3.2.1. Ni-based catalyst

As a low-cost and high activity, nickel is widely used in industry and one of the most studied metal. When ethanol reforming is considered Ni works well as it favors C-C bond cleavage. For example, Yang et al. [36] studied the activity of Ni catalysts supported on Al_2O_3, MgO, La_2O_3 and ZnO. They found that Ni/Al_2O_3 catalyst used at low temperature was faster deactivate than other catalyst due to ethylene formation on acidic size of Al_2O_3. The addition of alkali elements can decrease the acidity and the stability of catalyst increase. Ni/ZnO has the best catalyst performance among the catalysts [35]. Sun et al. studied H_2 production of Ni catalysts on different supports at

low temperature. The order of activity of their results as follow: $Ni/La_2O_3 > Ni/Y_2O_3 > Ni/Al_2O_3$. From their results, Ni/La_2O_3 has smaller Ni crystal grain lead to higher activity than other catalysts [37]. Fajardo et al. [36] studied the activity of Ni catalyst on various supports (Al_2O_3, MgO, SiO_2 and ZnO) in ethanol steam reforming for hydrogen production. Comparing the ethanol conversion and hydrogen selectivity over nickel-based catalysts, at 400°C of reaction temperature, the order of activity as follow: $Ni/SiO_2 >> Ni/Al_2O_3 > Ni/ZnO > Ni/MgO$. The Ni/SiO_2 catalyst is higher ethanol conversion than other catalysts, indicating that there is a higher amount of active sites usable for this catalyst. However, hydrogen selectivity was influenced by the support used in the following order: $Ni/SiO_2 \sim Ni/MgO > Ni/ZnO >> Ni/Al_2O_3$. The low H_2 selectivity presented by Ni/Al_2O_3 could be due to the great C_2H_4 formation promoted by this catalyst. In addition, according to the results, they conclude that at 400°C only Ni/SiO_2 was active in ethanol steam reforming and at 500°C of reaction temperature, Ni/SiO_2 and Ni/MgO showed activity for ethanol steam reforming [36]. The more extended study was performed by Duan and Senkan [38] for steam reforming of ethanol. They evaluated ZrO_2, CeO_2, TiO_2, SiO_2, Al_2O_3 supports by integrating most of the metals in the periodic table, using a combinatorial method. They concluded that Ni, Cu, Pd and Pt are among the most active metals in ethanol steam reforming reaction. In addition, they stated that copper was mainly predominant just in the first stages of the reaction mechanism namely ethanol dehydration and dehydrogenation steps whereas nickel was the phase mainly responsible for the hydrogen production although the copper presences decreased the CO and coke formation.

Among all metals, Rh and Ni produced the best activity and selectivity to H_2, and these metals favored the C-C bond cleavage in ethanol steam reforming [15]. Its ability to cleavage the C-C bond is demonstrated through the decomposition of ethanol on nickel surface [4]. The dissociation of ethanol proceeds via the scission of O-H in an ethoxide intermediate; the cleavage of C-H bond of the methylene group, resulting in the formation of acetaldehyde intermediate; and finally the breaking of C-C bond on the acetaldehyde intermediate, giving rise to adsorbed –CO and –CH_3 [39]. However, Rh metal was very expensive which is a major limiting factor in their use while Ni metal

was low cost. Thus, Ni-based catalysts has widely attention to use in ethanol steam reforming [40].

2.4. Electrospinning technique
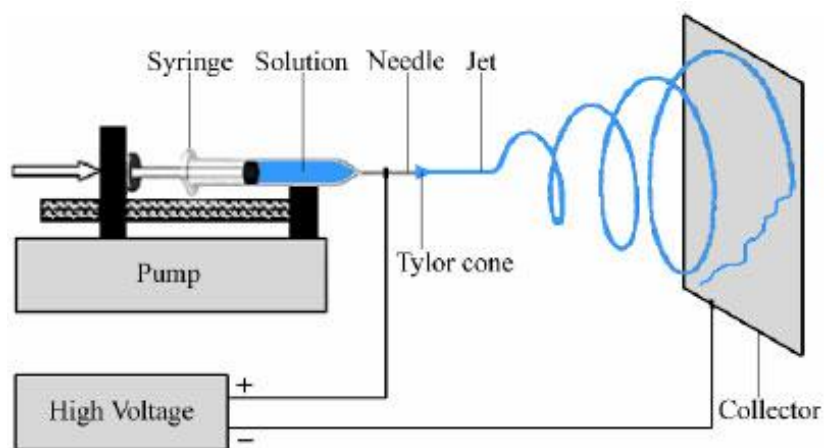
Figure 1 Schematic of polymer nanofibers production by electrospinning [41]

Electrospinning is a fiber production method that uses a high electrical field to draw a polymer melts or polymer solution into fine filaments. The basic electrospinning set-up, as shown in Figure 1, include a high voltage power supply, a needle nozzle, a container for spinning fluid and an electrode collector. When a polymer solution is charged with a high voltage, the electrostatic force draws the solution into a liquid jet. Because of the interaction between the jet and external electric field and charge repulsion inside the jet, the charged jet undergoes a bending or whipping instability to stretch taylor cone. Solvent evaporation from the filaments results in solid fibers (Figure 1). The elongation of the fiber as known from this bending in stability causes the formation of uniform fibers with nanometer scale diameters. An application for chemical catalyst of fiber structure prepared by electrospinning method is used to preserve increase activity of catalyst, high stability, and simplify the reaction process. An inert porous material with a large surface area and high permeability to reactants could be a promising candidate for efficient catalyst carriers.

Using an electrospun nanofiber combine with catalyst carrier, the greatly high surface can provide a large number of active sites, thus enhancing the catalytic performance. The well-interconnected small pores in the nanofiber mat warrant effective interactions between the reactant and catalyst, which is valuable for continuous flow chemical reactions. The catalyst can also be deposited onto the electrospun nanofiber surface via coating or surface modification.

2.5. Catalyst preparation

The activity of Ni/SiO_2 catalyst in ethanol steam reforming reaction is greatly influenced by the catalyst preparation method. Which is correlated to the number of active metals. There are several techniques of catalyst preparation method, such as impregnation [15], deposition-precipitation [42], strong electrostatic adsorption [18], co-precipitation [43] and colloidal [44].

2.5.1. Impregnation

The impregnation method is a widely used for preparing of silica supported metal catalysts. Two main impregnation methods are distinguished, namely, dry impregnation also called incipient wetness impregnation and wet impregnation. With dry impregnation, the mass of the oxide is high, and enough solution containing metal complex is added to simply "wet" the support. With wet impregnation metal solution is added in excess of the pore volume of the support material. The metal in solution is attracted to the support via interaction of physical adsorption. The impregnation method include three steps of preparation. The first step, the required amount of the metal precursor salt such as nickel(II) nitrate hexahydrate is dissolved in deionized water and added drop by drop to the support under constant stirring. After that, the sample is dried in an oven at 120℃ overnight to remove water. Finally, the catalyst is calcined in static or flowing air or pure oxygen at the proper temperature to remove the metal ligands and to reduce the metal to its catalytically active state [15]. There are several parameters can affect the properties of the obtained catalyst such as type of precursor, rate of the increasing temperature, and temperature of calcination. Impregnation method can prepare small particles of metal but difficult to obtain narrow particle size distribution, as shown in Figure 2.
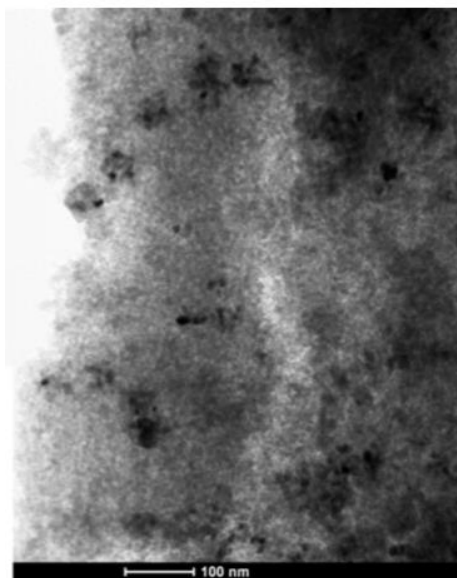
Figure 2 TEM image of Ni/SiO$_2$ prepared by impregnation method [17]

2.5.2. Strong electrostatic adsorption method

Strong electrostatic adsorption (SEA) is a catalyst preparation method which is based on basic concept of electrostatic attraction of oppositely charged particles. A landmark work is the postulation of Brunelle that the adsorption of noble metal complexes onto common oxides supports was essentially coulombic in nature [16]. Silica and other metal oxides contain hydroxyl groups on its surface. Point of zero charge (PZC) is the pH value of a medium where the hydroxyl groups on the surface of the support remain neutral. In a pH<PZC medium, the hydroxyl groups will be protonated and become positively charged and thus attracting anions such as hexachloroplatinate. When pH>PZC, the hydroxyl groups will deprotonate and became negatively charged and attracting cations such as nickel tetraammine. A simple intuitive picture of this surface chemistry is presented in Figure 3. In other words, pH value plays an important role in the deposition of metal precursor. The SEA method was able to produce nanocatalyst of spherical-shaped nickel nanoparticles on SiO$_2$ support as shown in Figure 4, with Ni average size of 3 nm [18].
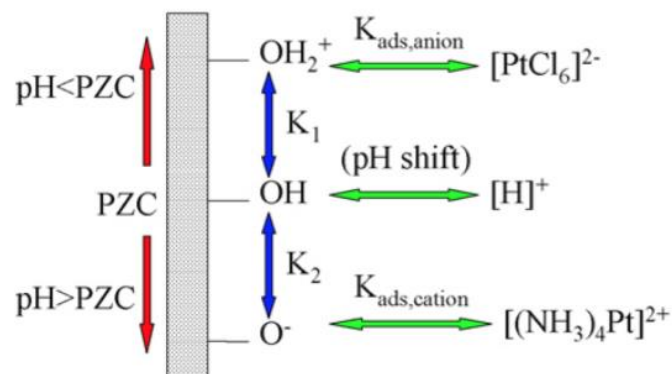
Figure 3 Mechanism of electrostatic adsorption [18]
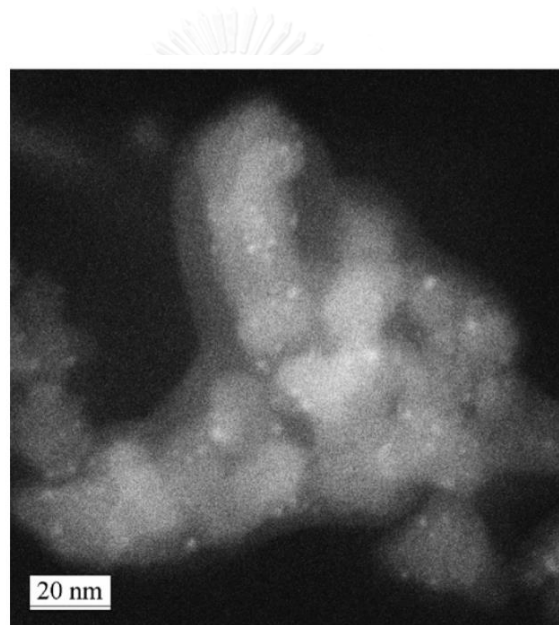
Figure 4 TEM image of 1.6 wt% Ni/SiO_2 prepared by SEA method [18]

2.5.3. Deposition precipitation method

Deposition precipitation concerns deposition from a precursor solution through a change of pH, temperature, or evaporation, so that metal compounds are formed with a low solubility, often metal hydroxides. In the case of deposition precipitation, this is done in the presence of an existing support, and the concentration of the new compound is increased gradually to prevent formation of bulk phases in solution. Preferential precipitation on the support can be achieved because introduction of the

support in the solution causes either a reduction of the surface free energy of tiny nuclei or stabilization of the precipitate, decreasing the energy barrier for nucleation. Hence, conditions exist where nucleation can only occur on the support and not in the bulk solution, so that the support surface functions as a seed for nucleation [45]. Nucleation of the metal species is generally induced by changing the pH so compounds with a low solubility are formed. When this is done by injection of the precipitant (e.g., alkaline solution), great care has to be taken to prevent local concentrations exceeding the critical supersaturation, which would cause bulk precipitation. Because of this, homogeneous deposition precipitation methods are often preferred, whereby precipitation is induced homogeneously throughout the reaction vessel. This can be achieved by adding urea (at room temperature), which when heated to 90°C will slowly decompose, resulting in the formation of OH^-, thereby slowly enhancing the pH upon decomposition. Other popular precipitation techniques include the direct reduction of solvated metal ions to the metal or a gradual reduction of the pH by slow removal of ligands such as ammonia via evaporation. Classically, deposition precipitation was developed to produce catalysts with metal loadings that exceed those obtained by impregnation which is limited by solubility [46].
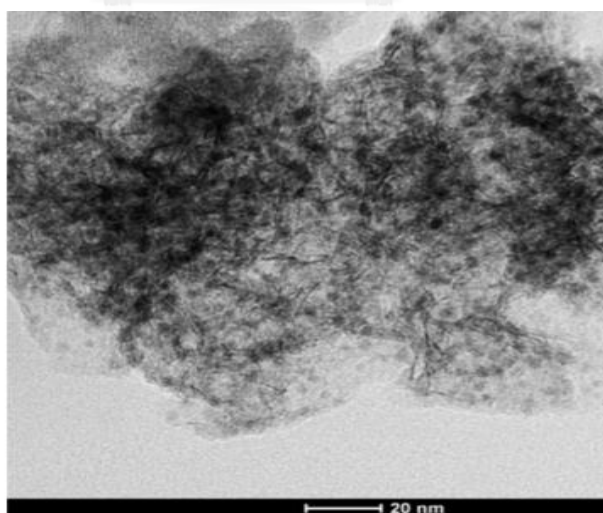
Figure 5 TEM image of 10 wt% Ni/Ai_2O_3 prepared by DP method [17]

2.5.4. Co-precipitation method

In this method, salts of the support and active metal are dissolved and mixed with basic reagent, generally alkali hydroxides or carbonates. Then, precipitation the hydroxides or carbonates of support and the active metal are formed. After that, these precipitates are filtered, washed, dried and calcined. Sodium carbonate and potassium carbonate are widely used to adjust the pH during this process. While, carbonate and sodium hydroxide improve the stability of pH. Using co-precipitation method Ni on Al_2O_3 [43], CeO_2 [47] can be prepare with high dispersion. However, during precipitation, had to prevent local fluctuations in the conditions caused by, for example, temperature gradients, insufficient mixing, or concentration gradients, which can cause additional nucleation events, different or inhomogeneous growth patterns, or the precipitation of different phases.
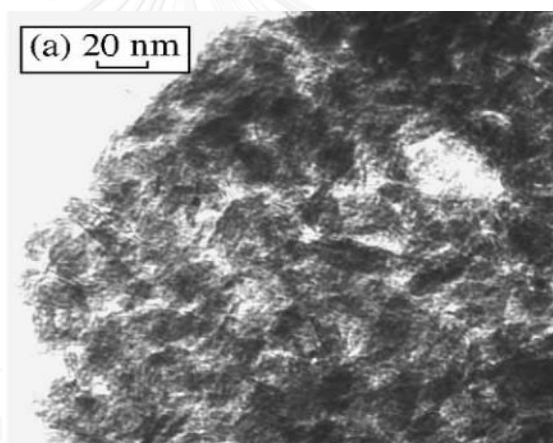
Figure 6 TEM image of 10 wt% Ni/Ai_2O_3 prepared by co-precipitationl method [43]

2.5.5. Colloidal method

Colloidal synthesis is a preparation method that can synthesis nanosized catalyst by using stabilizer in order to control particle size and composition of catalyst. Typically, catalyst are added into solution which contains a solvent with dielectric constant, then a colloid forms in solution. The catalyst particles are absorbed by the ionomer colloid and then ionomers link continuous network resulting in catalyst layers formation. The polyol process are applied produce nanosized catalyst and modified coordination capture as same as colloidal method. For example, the monodispersed

iron nanoparticles were prepared by the alcohol reduction of iron (III) acetylacetonate at high temperature [48]. In the colloidal method, the surfactant- stabilized colloids is essential to disperse and stabilize nanoparticles in the solvent. The colloidal method had prepared high dispersion of iron nanoparticles with average size of 10 nm, as depicted in Figure 7.
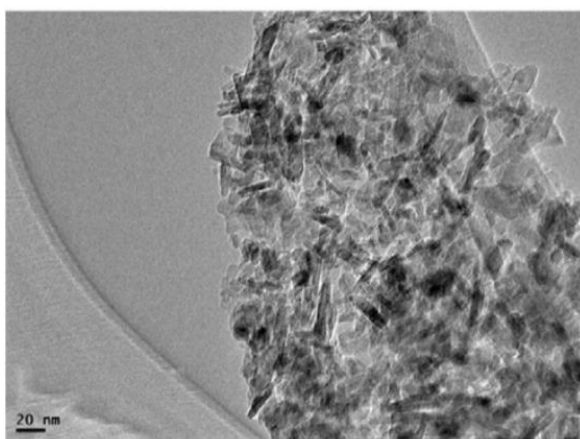
Figure 7 TEM image of 10 wt% Ni/Ai$_2$O$_3$ prepared by polyol method [44]
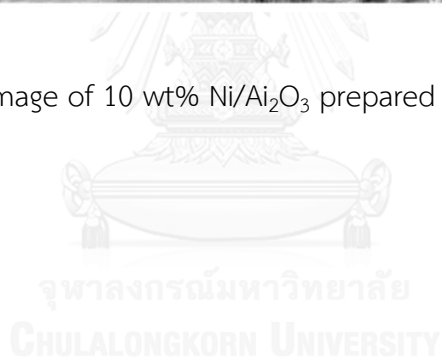
2.6. Literature review

Gayubo et al. [49] prepared Ni and Co supported on SiO_2 and Al_2O_3 catalysts in order to compare the catalyst performance in ethanol steam reforming. Their results showed that Ni catalyst had higher ethanol conversion than that of Co catalyst. This was explained its higher capacity of breaking C-C bond. Also, the Ni supported on SiO_2 catalyst had a higher activity than supported on Al_2O_3 catalyst. In addition, they found that the addition of La_2O_3 gave way to increase ethanol conversion and H_2 selectivity also.

Vicente et al. [20] studied the effect operating conditions (steam/ethanol molar ratio, temperature, and space time) of Ni/SiO_2 catalyst in ethanol steam reforming. From their result, the Ni/SiO_2 gave total ethanol conversion with a steam/ethanol molar ratio of 6 at above 500°C and a space time of 0.138 $g_{catalyst}\cdot h/g_{ethanol}$. Moreover, The formation of coke at 300°C was amorphous which could be block the metallic sites, while at higher temperature the formation of coke was mainly carbon nanofiber. In addition, above 600°C the coke content was decreased due to gasification reaction.

Frustery et al. [50] focused on ethanol steam reforming over Ni-based catalyst which different supports (MgO and CeO_2). The Ni/MgO and CeO_2 catalysts were efficient systems for H_2 production at high temperature. Both catalytic systems, at equilibrium conditions, were able to produce an H_2 selectivity of 76% at 650°C. Addition of H_2O to the $EtOH/H_2O$ reaction stream was crucial in avoiding catalyst deactivation of both catalytic systems.

Monica Dan et al. [51] reported ethanol conversion at low temperature and high steam/ethanol molar ratio over Ni catalysts coated on La_2O_3 or CeO_2 deposited on Al_2O_3 and ZrO_2. They concluded that the excess amount of water enhanced the steam reforming of ethanol while decreasing the carbon formation. Moreover, the addition of ZrO_2 and La_2O_3 increased the yield of hydrogen. For Ni/La_2O_3-ZrO_2 was giving the highest conversion of ethanol and hydrogen yield. 100% ethanol conversion and 55% of hydrogen yield were obtained. All catalysts over Ni promoted on zirconia support were stable in 24 h with time on stream.

Lindo et al. [52] prepared Ni supported on Al-SBA-15 mesoporous catalysts in order to study the effect of Al incorporation on property and performance of catalyst

in steam reforming of ethanol reaction. They was found that several properties such as ordering of meso structure, acidity, nickel dispersion and metal-support interaction of Ni/SBA depend on the ratio of Si/Al in SBA-15 structure. Ni/Al- SBA-15 catalyst showed large Ni particles size and strong metal-support interaction. All of catalyst were active in steam reforming of ethanol and selective to hydrogen, but although Ni/Al-SBA catalysts gave almost 100% conversion of ethanol for Si/Al ratios lower than 60, this presented lower selectivity to main products. The Al doped in SBA-15 mesoporous support was responsible for the acid sites formation of catalyst; therefore Al has a positive effect on the distribution of product. Acid sites of support enhanced dehydration of ethanol leading to higher coke deposition. Thus, the best catalytic results, in terms of highest H_2 selectivity and lower carbon formation, were reached on Ni/SBA-15 catalyst.

Kraikeaw et al. [53] studied the optimum parameter for synthesis of silica fibers using the sol–gel method and electrospinning technique. The silica fibers were successfully synthesized by electrospinning technique and the optimized condition was TCD 15 cm and applied voltage 15 kV to produce continuous and submicron fibers with a diameter of 0.83 μm.

Reubroycharoen et al. [54] prepared Ni/SiO$_2$ fiber catalyst via impregnation method in order to study the effect of supported shape on activity of catalyst in glycerol steam reforming. They found that the conversion of glycerol over the fiber catalyst was higher than that over the porous catalyst. Also, the glycerol conversion of the Ni/SiO$_2$ fiber catalyst become equilibrium faster than that of the Ni/SiO$_2$ porous catalyst.

Kim et al. [55] compared the activity of Pt/TiO$_2$ fiber and Pt/TiO$_2$ bulk catalysts in water gas shift reaction. Their results shown that the fiber catalyst had high activity and stability than bulk catalyst because the Pt on surface of fiber catalyst provided easily accessible to reactants. Moreover, the fiber catalysts could be reduced at lower temperature than bulk catalysts.

Jiao et al. [18] studied the uptake of cationic metal complexes (i.e., [Pd(NH$_3$)$_4$]$^{2+}$, [Cu(NH$_3$)$_4$]$^{2+}$, [Co(NH$_3$)$_6$]$^{3+}$, [Ru(NH$_3$)$_6$]$^{2+}$, [Ru(NH$_3$)$_6$]$^{3+}$ and [Ni(NH$_3$)$_6$]$^{2+}$ over amorphous silica support at high pH. The sample catalysts prepared by strong electrostatic

adsorption (SEA) method were compare with the impregnation method. They found that the catalyst prepared by SEA method had a smaller particle size and higher dispersion of metal catalyst than that prepared by impregnation method at the same metal loading. Moreover, for the same preparation method, the dispersion of metal on surface of amorphous silica decreased with increasing of metal loading at the same calcination temperature. Calcination at high temperature caused sintering of metal over the amorphous silica support and lead to lower dispersion.

Bertone et al. [17] studied the effect of preparation methods over Ni catalyst supported on silica and alumina in gas-phase hydrogenation of maleic anhydride. The Ni-base catalyst prepare by deposition precipitation method (PD) was compared with impregnation method (I). They found that the interaction between nickel oxide and the support strongly depends on the preparation method. The order of metal support interaction was as follows: Ni/SiO_2-PD >Ni/SiO_2-Al_2O_3-PD >Ni/SiO_2-I. The Ni/SiO_2-PD catalyst prepared by deposition precipitation presented small particle size and strong metal- support interaction and improved the catalyst activity.

CHAPTER III

EXPERIMENTAL

3.1. Matherial and reagents

The chemical materials were used in this study were listed in Table 1.

Table 1 List of chemicals and sources

Chemicals	Source
Nitrogen gas (99.99% purity)	Praxair
Hydrogen gas (99.99% purity)	Praxair
Air zero gas (99.99% purity)	Praxair
Helium gas (99.99% purity)	Praxair
Standard gas (1% CO, 1% CO_2 1% CH_4 and 1% H_2 within 96% N_2)	Praxair
Nickel nitrate hexahydrate ($Ni(NO_3)_3 \cdot 6H_2O$)	Sigma-Aldrich
Tetraethyl orthosilicate (TEOS; $Si(OC_2H_5)_4$, 95 % A.R. Grade)	Sigma-Aldrich
Silica (Q-10)	Sigma-Aldrich
Ammonia solution (27%, A.R. Grade)	Sigma-Aldrich
Nitric acid (HNO_3, 69 wt% A.R. Grade)	Sigma-Aldrich
Hydrochloric acid 37 wt%	Sigma-Aldrich
Ethanol	Sigma-Aldrich
quartz sand	Herosign

3.2. Catalysts preparation

Ni-supported on porous silica (SP) and silica fiber (SF) catalysts were prepared by impregnation (IM), deposition precipitation (DP) and strong electrostatic adsorption (SEA) methods.

3.2.1. Preparation of Silica fiber

The silica sol solution was prepare as the following procedure: First, TEOS (1 mole) was dissolved in distilled water (2 mole). Then, HCl (0.01 mole) and ethanol (2 mole) were added to the solution under stirring for each step for 5 min. After that, the solution was stirred at 55°C for 50 min. Finally, the solution was cooled to room temperature [53]. The silica fibers were prepared by electrospinning process. Electrospinning was performed with an equipment (Figure 8). A clamp connected with high voltage power supplier which was connected to the syringe. The needle to collector distance (TCD) was 15 cm. The silica sol solution was loaded into a syringe which was attached to spring pump. The feed rate at 10 mL/h and potential of 15 kV were applied to the needle. The electrospun fibers were collected, and then dried at 110°C overnight and calcined at 500°C for 2 h [54].
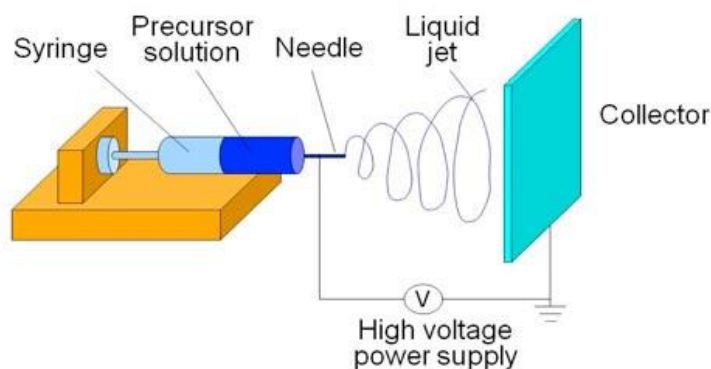
Figure 8 Schematic of the electrospinning process setup [41]

3.2.2. Preparation of Ni supported on silica catalysts

The Ni/SiO$_2$ catalysts (The Ni loading was 10% in all cases) were prepared by wetness impregnation (IM), strong electrostatic adsorption (SEA), deposition precipitation (DP). The samples named Ni/SP–IM and Ni/SF–IM were prepared by impregnation method. The IM samples were prepared as the following procedure: Ni(NO$_3$)$_2$·6H$_2$O was dissolved in DI water and then, this solution was added drop by drop to the support. The DP sample was prepared the following procedure:

$Ni(NO_3)_2 \cdot 6H_2O$ was dissolved in DI water and ammonia solution (28 wt%) was added slowly to adjust pH to 9. Then silica fiber was put in precursor solution to stare DP of Ni on silica fiber at room temperature. After 12 h DP time, the solid was filtrated and washed with DI water. The SEA samples were prepared the following procedure: silica fiber was added to DI water and adjusted pH to 12 by using ammonia solution (28%). After that, the solution was added into the mixture. Then, the solid was filtrated and washed with DI water until pH 7. All the catalysts were dried at 120°C for 12 h and calcined at 500°C for 2 h.

3.3. Catalysts characterization

3.3.1. Nitrogen adsorption-desorption measurement

The specific surface areas and pore size of catalyst sample were measured in Quantachrom (AUTOSORB 1) at liquid nitrogen temperature (-196°C). Prior to analysis, the catalysts were degassed and heat at 200°C for 2 h. The specific surface areas were estimated by Brunauer- Emmett-Teller (BET) equation and the pore volume and mean pore diameter were calculated by the Barrett-Joyner-Halenda (BJH) method.

3.3.2. Energy dispersive X-ray analysis (EDX)

The determination of the amount of metal in catalyst samples were measured using energy dispersive X-ray analysis (EDX) on a Rayny EDX-700 instrument.

3.3.3. Temperature-programmed reduction (H_2-TPR)

Temperature-programmed reduction (H_2-TPR) was carried out by handmade machine to analyst the reduction of metal oxidation state. The catalyst sample was pretreated with nitrogen flow at 100°C for 30 min to remove trace of water. After that, the catalysts was exposed to reduce in 5% hydrogen in nitrogen ($5\%H_2/N_2$) while the temperature was increased up to 900°C at the rate of 10°C/min. Schematic of temperature program of H_2-TPR measurement was presented in Figure 9. The H_2 consumption was monitored by gas chromatography thermal conductivity detector (GC-TCD).
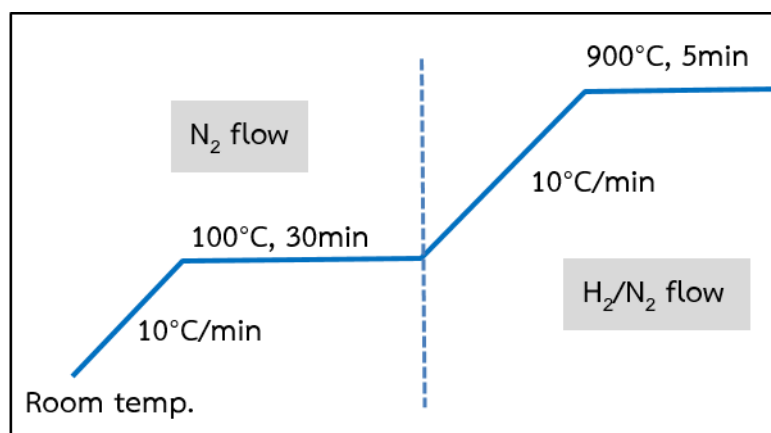
Figure 9 Schematic of temperature-program of H_2 TPR

3.3.4. X-ray diffraction (XRD)

X-ray diffraction (XRD) was performed to examine the crystal structure and particle size of catalysts at room temperature in a Bruker D8 Advance equipped with Cu-K$_\alpha$ radiation. The profile was scanned in the 2 degree (2θ) range of 5°- 80° at 0.02 steps. The mean particle size of NiO catalysts after calcination was estimated by the Scherrer's equation at the (2 0 0) diffraction plane (2θ=43.5°).

3.3.5. Scanning electron microscopy (SEM)

The morphology of all catalysts were obtained using a Field Emission Scanning Electron Microscope and Energy Dispersive X-Ray Spectrometer (FESEM-EDS) of JSM-7610F model.

3.3.6. Transmission electron microscopy (TEM)

The nickel oxide particle size and the dispersion of nickel on silica fibers support with different preparation methods were observed by using a FEI Tecnai G^2 20 TEM/STEM/EDX transmission electron microscope operated at 200 kV.

3.3.7. Thermogravimetric analysis (TGA)

Thermogravimetric analysis was used to estimate the coke on spent catalyst. It were carried out in TGA/DSC 1 (Mettler Toledo) instrument. The TGA/DSC was performed by ramping the sample temperature at 10.2°C/min from 50 to 600°C. Then, the temperature was increased up to 1000°C with the rate of 4.8 °C /min and holding time for 20 min. Schematic of temperature program for TGA measurement was shown in Figure 10.
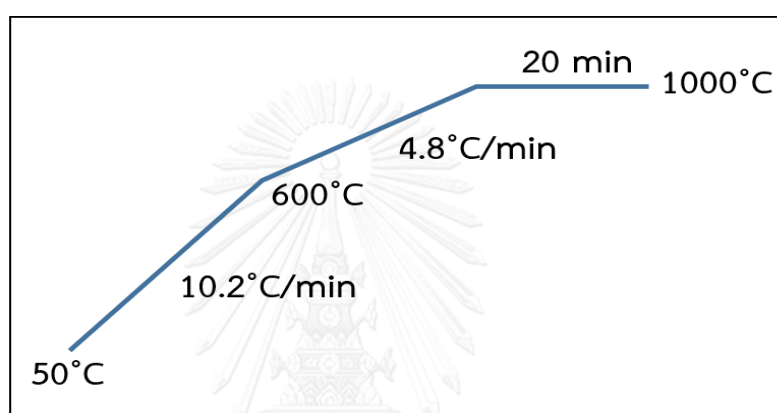
Figure 10 Schematic of thermogravimetric analysis

3.4. Catalyst performance in ethanol steam reforming

The catalyst performance in ethanol steam reforming was carried out in a fixed-bed reactor. Prior to the test, the catalysts were reduced at 700°C online for 1 h in a flow of 10 vol % H_2/N_2 (50 mL/min). The reaction conditions were performed at temperature range of 400 to 600°C, pressure of 1 atm, 0.2g catalyst, reaction time of 6 h, water/ethanol of 9:1 (molar ratio), and feed rate (water/ethanol) of 0.04 mL/min through HPLC pump into a heated chamber at 150°C to evaporate the solution completely in the stream of N_2 of 20 mL/min. The product were analyzed by on-line GC-FID-TCD equipped with Porapak-Q column [56].
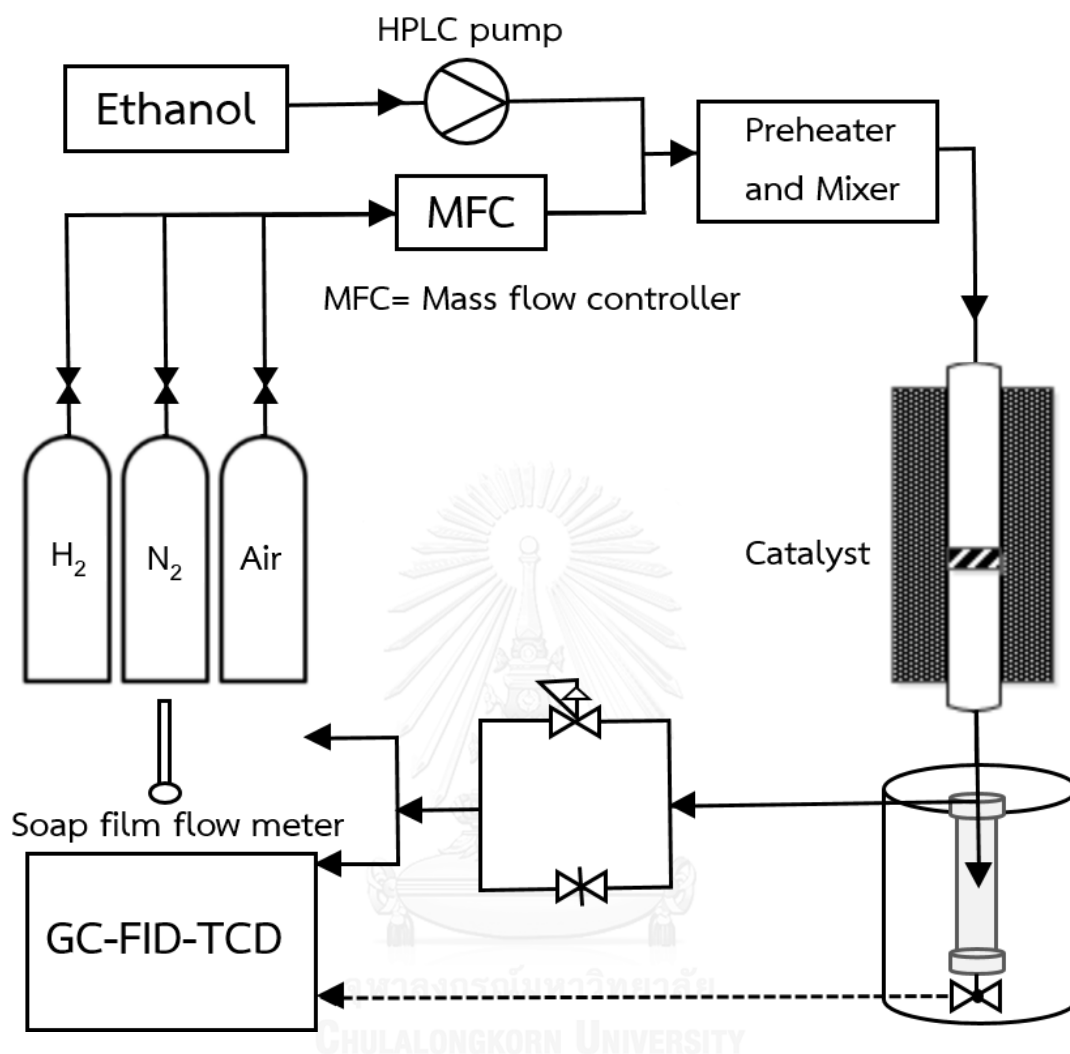
Figure 11 Reactor system for Ethanol Steam Reforming

Product analysis

The effluent gas from fixed-bed reactor was detected online by gas chromatograph (Shimadzu GC 14B). While CO, CO_2, H_2 and N_2 were analyzed by thermal conductivity detector (TCD) and the hydrocarbon gas were analyzed by flame ionization detector (FID) with Porapak Q column.
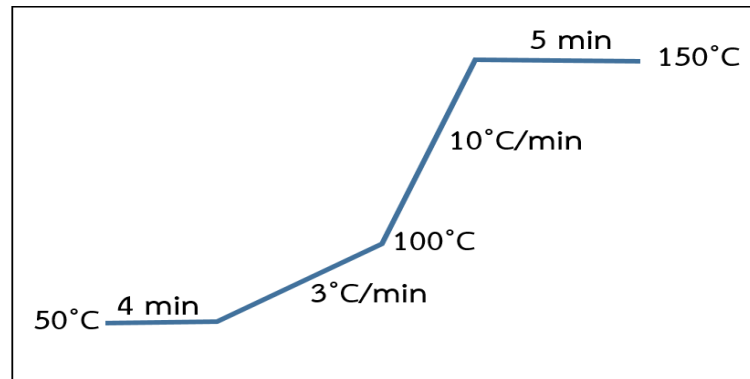
Figure 12 GC heating program for gas analysis

The results were reported in terms of ethanol conversion, selectivity to products and

hydrogen yield, defined as follows (Eqs. :1-3)

$$X_{(ETOH)} = \frac{F_{in} - F_{out}}{F_{in}} \times 100 \qquad (1)$$

When $\quad$ $X_{(ETOH)}$ = ethanol conversion

$\quad$ F_{in} = molar flow rate of ethanol inlet

$\quad$ F_{out} = molar flow rate of ethanol outlet

$$S_{(i)} = \frac{F_{C_i}}{F_{C_{out}}} \times 100 \qquad (2)$$

Where $\quad$ $S_{(i)}$ = selectivity of product gas

$\quad$ F_{C_i} = molar flow rate of the carbon containing species (i) in the products,

including CO, CO_2, CH_4, C_2H_4, C_2H_6 and CH_3CHO

$\quad$ $F_{C_{out}}$ = molar flow rate of C atom total in gas outlet

$$Y_{H_2} = \frac{F_{H_2}}{6\, F_{in}} \times 100 \qquad (3)$$

When $\quad$ Y_{H_2} = hydrogen yield

$\quad$ F_{H_2} = molar flow rate of the hydrogen product

CHAPTER IV

RESULTS AND DISCUSSION

4.1. Catalytic characterization

4.1.1. Nitrogen adsorption-desorption

The textual properties, including BET surface area, pore volume, average pore diameter of support and nickel-based catalyst as well as Ni content and NiO crystallite size were presented in Table 2.

Table 2 Textural properties of the different nickel catalysts

Samples	S_{BET} (m^2/g)	Vp (cm^3/g)	Dp (nm)	Ni content [a] (%)	NiO crystal size [b] (nm)	NiO crystal size [c] (nm)
SP	236.3	1.161	12.4	-	-	-
SF	5.9	0.001	10.2	-	-	-
Ni/SP-IM	240.2	1.167	12.7	11	15	13
Ni/SF-IM	9.9	0.011	10.3	11	22	20
Ni/SF-DP	26.7	0.028	5.8	11	14	13
Ni/SF-SEA	35.9	0.029	5.9	8	7	7

[a] Ni content was analyzed by the EDX technique.

[b] The crystallite size of NiO was calculate by the Scherrer's equation.

[c] The crystallite size of NiO was calculate by TEM image.

The BET surface area of silica porous (SP) support (236 m^2/g) was much higher than silica fiber (SF) support (6m^2/g). Figure 13 show the N_2 adsorption-desorption curves of SP and SF supports. The SP support exhibited type IV isotherm that implied mesoporous structure [57] Instead, the isotherm of SF support showed adsorption isotherm III [53], which indicated non-porous structure. Moreover, Figure 14 present N_2 adsorption-desorption curves of the Ni-base catalysts on SF support were prepared by the different methods.
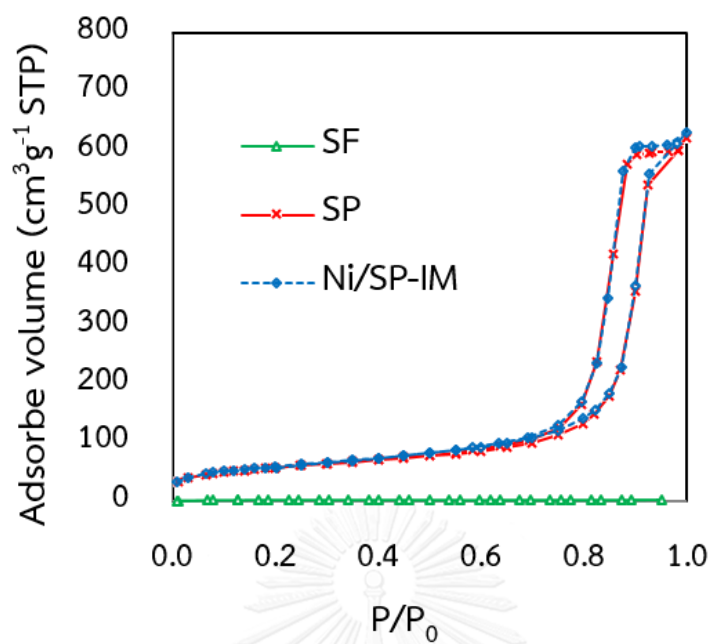
Figure 13 N_2 adsorption-desorption isotherms of calcined support (SP and SF) and
catalyst (Ni/SP-IM)
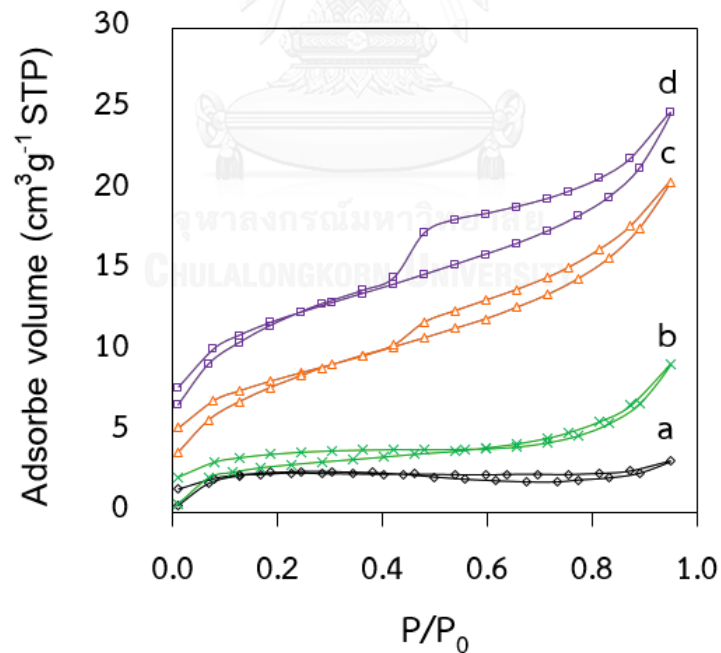
Figure 14 N_2 adsorption-desorption isotherms of catalysts: (a) SF, (b) Ni/SF-IM,
(c) Ni/SF-DP and (d) Ni/SF-SEA

The Ni/SP-IM, Ni/SF-IM, Ni/SF-DP and Ni/SF-SEA catalysts had higher N_2 adsorption capacity than both supports, which indicated the NiO particle covering on surface of SF support. The Ni/SF-IM catalyst had the lowest BET surface areas (9.9 m^2/g) because the NiO particle could be easy to aggregate and lead out in the calcination step [44]. The Ni/SF-SEA catalyst had high BET surface areas (35.9 m^2/g) because the SEA method provide high dispersion of nickel on the support surface [18]. Moreover, The actual nickel content of Ni/SF-SEA was slightly lower than the theoretical value. Whereas, the actual nickel contents of others catalyst was be nearly equal to the theoretical value. Thus, the nickel was deposited on the support successfully.

4.1.2. X-ray diffraction (XRD)

The XRD pattern of the different nickel catalysts were presented in Figure 15.
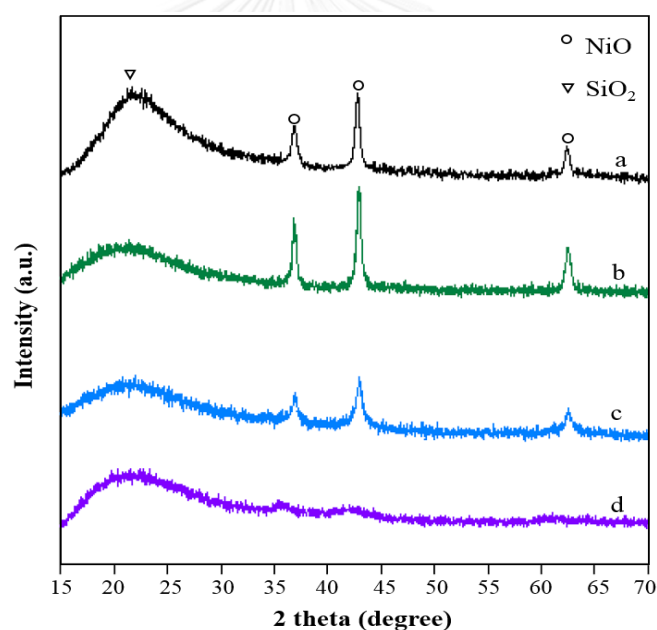
Figure 15 X-ray diffraction patterns of the calcinated catalyst: (a) Ni/SP-IM, (b) Ni/SF-IM, (c) Ni/SF-DP and (d) Ni/SF-SEA.

X-ray diffractometry (XRD) was performed to identify the crystalline structure by their diffraction patterns. It has been presented that the crystal with a particular set of atomic planes oriented toward the X-ray beam diffracts X-rays at an angle zeta determined by the distance between the planes.

The XRD pattern of catalysts sample after calcination at 500°C for 2 h was presented in Figure 15. The NiO phase showed peak at 2 theta of 37.3°, 43.2°and 63.0° corresponding to crystal plane of (1 0 0), (2 0 0) and (2 2 0) respectively [58, 59]. A broad peak around 22 was attributed to amorphous silica [14, 54]. The crystallite size was summarized in Table 2. The size of NiO particles calculated by the Scherrer equation from the NiO (2 0 0) crystal plane was 15 nm for Ni/SP-IM, 22 nm for Ni/SF-IM, 7nm for Ni/SF-SEA, and 14 nm for Ni/SF-DP. The NiO peak of Ni/SF-SEA prepared by strong electrostatic adsorption method were broad, a smaller particle size as well as dispersion than catalyst obtained by impregnation and precipitation–deposition methods, lead to high catalytic activity in ethanol steam reforming.

4.1.3. Temperature-programmed reduction (H$_2$-TPR)
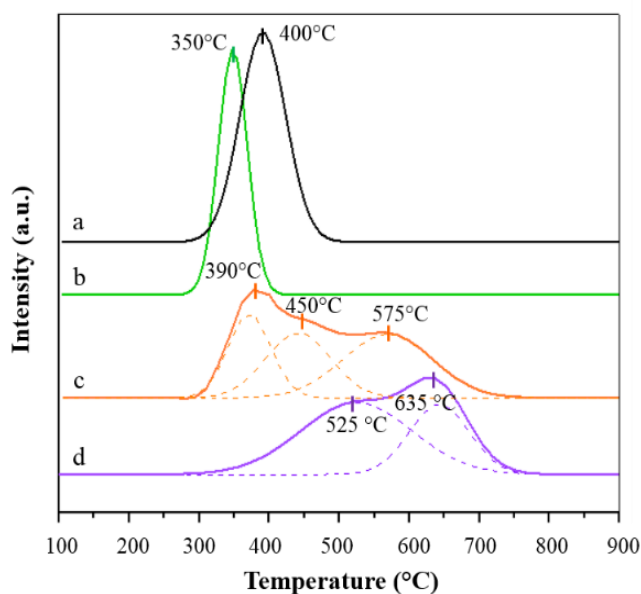
Figure 16 Temperature-programmed reduction profile of catalysts sample: (a) Ni/SP-IM, (b) Ni/SF-IM, (c) Ni/SF-DP and (d) Ni/SF-SEA. Inside peak was analyzed by Origin-Lab program.

The H$_2$-TPR analysis was performed to determine the reducibility and the optimum reduction temperature of catalysts for the ethanol steam reforming. The H$_2$-TPR profiles of the catalysts sample was shown in Figure 16 (a-d) for catalysts prepared by impregnation, deposition precipitation and strong electrostatic adsorption. The reduction peak correspond to the reduction of NiO to Ni^0. For the Ni/SP–IM and Ni/SF–

IM catalysts, the reduction peak between 350℃ and 400℃ were observed. The presence of these peak had indicated low temperature peak of NiO that weak interaction between catalyst and support [14, 54]. However, in the case of impregnation catalyst, the fiber catalyst required a lower reduced temperature than porous catalyst, indicating that the NiO particle size of Ni/SP-IM was smaller than Ni/SF-IM. These results were agreement with XRD result. Moreover, the TPR pattern of the impregnation catalysts showed narrow peak, while, the catalyst prepared by DP and SEA methods presented very broad peaks. The Ni/SF-DP catalyst showed three broad peaks. The first peak at around 390℃ indicating large particles of NiO. The peaks between 450℃ and 575℃ were assigned to either small particles of NiO that strongly interacted with the support [17, 60]. For Ni/SF-SEA catalyst, the reduction peak was observed in the range of 525 and 635℃ leading to stronger resistance to sintering and deactivation of catalyst [18]. Thus, the metal-support interaction were ordered by Ni/SF-SEA > Ni/SF-DP > Ni/SP-IM > Ni/SF-IM.

4.1.4. Scanning electron microscopy (SEM)

The morphology of the SF support and the different Ni/SF catalysts were analyzed by scanning electron microscope. Figure 17(a) presented smooth surface morphology of SF support. The surface morphology of fresh catalysts showed the NiO particle deposition on the surface of SF support and the deposition of NiO was influenced by catalyst preparation methods as shown in Figure 17(b-d). The Ni/SF-IM catalysts prepared by impregnation method presented poor distribution of nickel oxide particle on the surface of silica fibers. Moreover, the particle size of NiO was larger than other catalysts. While the most past of NiO particle of the catalyst prepared by deposition precipitation was small size but there was large NiO particle size in some part on the surface of silica fibers. On the other hand, the Ni/SF-SEA catalyst prepared by strong electrostatic adsorption was good distribution and small size of NiO particle on the SF surface as a result from strong metal-support interaction [18, 53]. SEM result was well agreement with the TEM images as shown in Figure 18.
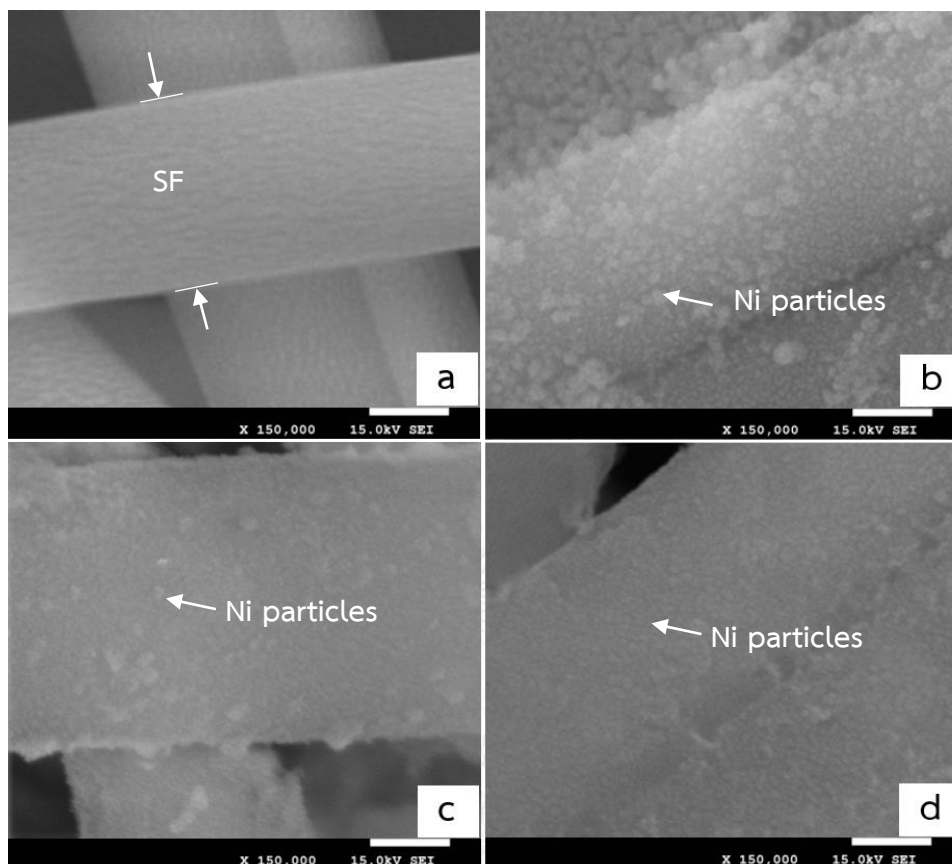
Figure 17 SEM micrographs of the calcinated catalysts: (a) Ni/SP-IM, (b) Ni/SF-IM,
(c) Ni/SF-DP and (d) Ni/SF-SEA.

4.1.5. Transition electron microscopy (TEM)

TEM micrographs of the different catalysts after calcination were shown in Figure 18. The NiO particles were the darker point while the SP and SF were lighter ones. All catalysts appeared spherical shapes of NiO particle decoration on the silica support. The NiO particles of Ni/SP-IM were well dispersed than Ni/SF-IM due to difference of support shape. In addition, the NiO particle size was influenced by the preparation method as compared in Figure 18(b-d). From Figure 18(d), the Ni/SF-SEA catalyst prepared by SEA method had the best NiO dispersion as well as smallest NiO particle size (7 nm), implying that the SEA method was most suitable for deposition of NiO on SF support. The particle size of NiO calculated from TEM images were in the range of 7-22 nm as presented in Table 2. The mean particle size of NiO were ordered

by Ni/SF-SEA < Ni/SF-DP < Ni/SP-IM < Ni/SF-IM, which was well consistent with the XRD analysis as shown in Figure 17 and Table 2.
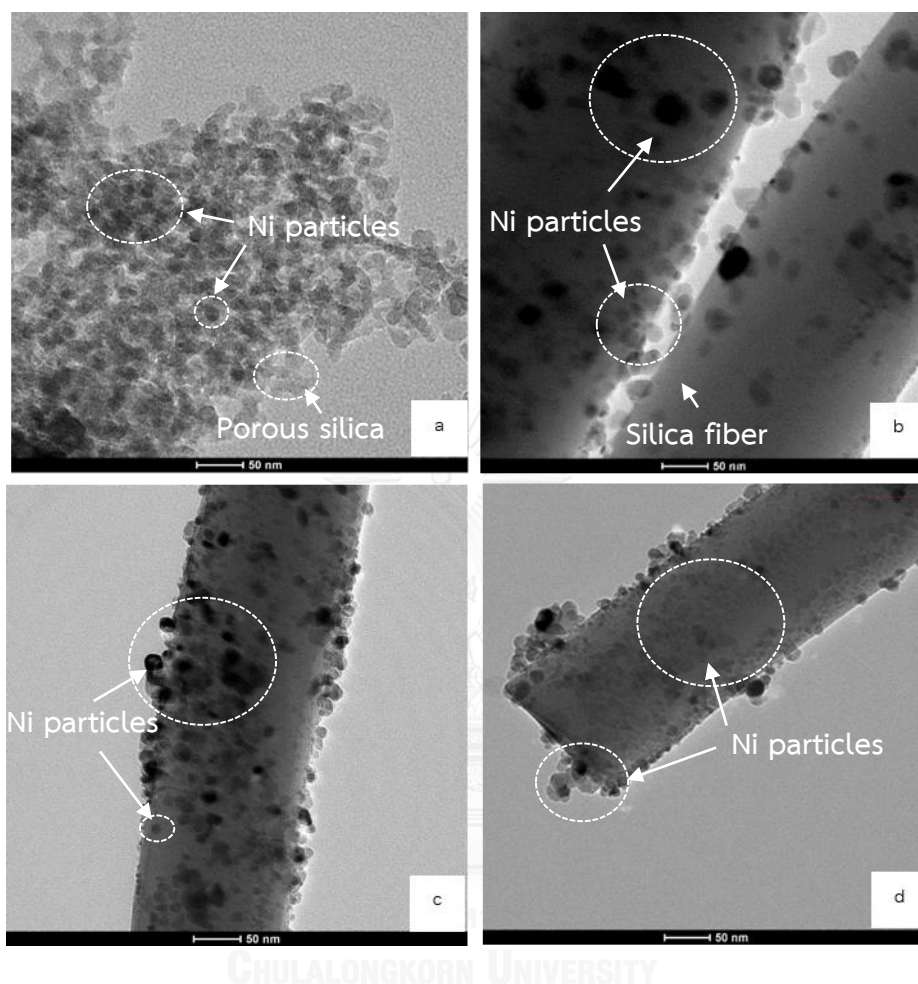
Figure 18 TEM micrographs of the calcinated catalysts: (a) Ni/SP-IM, (b) Ni/SF-IM, (c) Ni/SF-DP and (d) Ni/SF-SEA.

4.2. Catalytic performance of Ni-base catalysts in ethanol steam reforming

4.2.1. Effect of shape support: porous and fiber
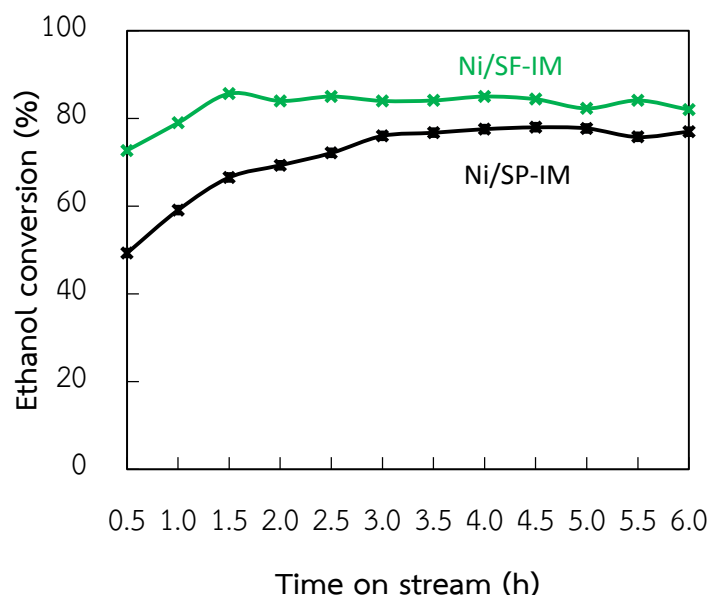
Figure 19 Ethanol conversion with time on stream over Ni/SP-IM and Ni/SF-IM catalysts at 400°C, S/E: 9:1, W/F: 18 g_{cata}·h/mol$_{ethanol}$.

The effect of shape support of catalysts on ethanol conversion was illustrated in Figure 19. Only gas products were collected on carrying out the catalytic tests with a H_2O/EtOH molar ratio of 9 and 18 $g_{catalyst}$·h/gmol$_{EtOH}$ space time at 600°C. Ethanol conversion over porous catalyst (Ni/SP-IM) was slightly lower than that of fiber catalyst (Ni/SF-IM) because the porous catalysts have limit diffusion of reactants and products, resulting in the decrease in catalyst performance. However, Ni/SF-IM catalyst was faster arriving equilibrium than that porous catalyst. Moreover, Ni/SP-IM catalyst had higher coke formation than Ni/SF-IM catalyst (Figure 29.). It has been reported that carbon formation can block active Ni, resulting in low catalytic performance [20, 61].

Figure 20 shows H_2 yield and selectivity of products, i.e. CO, CO_2, CH_4, C_2H_6, C_2H_4 and C_2H_4O in outlet steam with different shape of catalysts at 400°C with a H_2O/EtOH molar ratio of 9 and 18 $g_{catalyst}$·h/mol$_{EtOH}$ space time. The H_2 content about 17% was observed over the Ni/SF-IM catalyst, while 13% H_2 selectivity was achieved on the Ni/SP-IM catalyst.
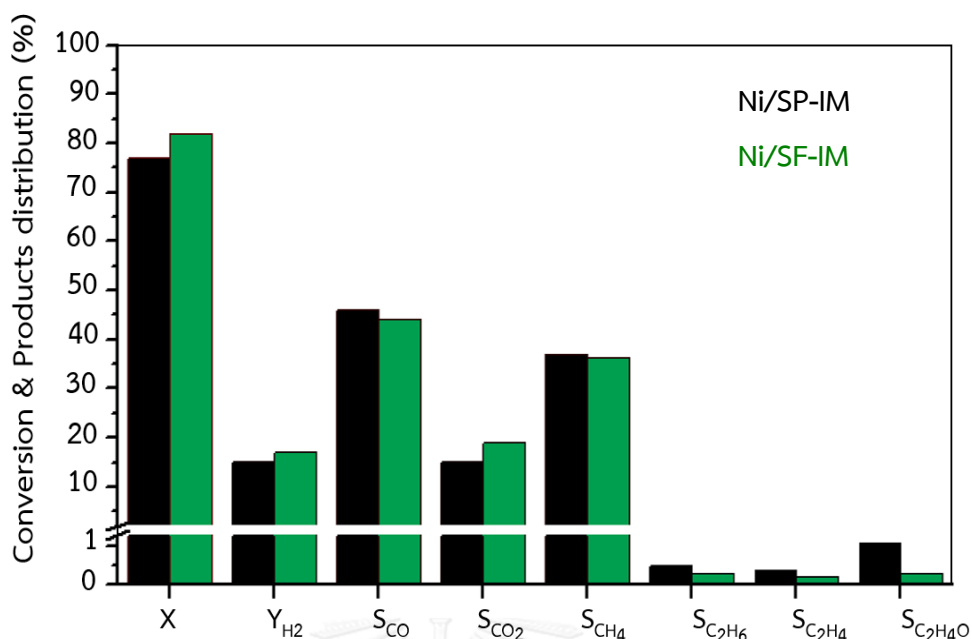
Figure 20 ESR activity over Ni/SP-IM and Ni/SF-IM catalysts at 400°C, S/E: 9:1, W/F: 18 $g_{cata.} \cdot h/mol_{ethanol}$ within 6 h.

The H_2 yield and CO_2 selectivity on Ni/SF-IM catalyst were higher than Ni/SP-IM catalyst; whereas CO selectivity and CH_4 selectivity on Ni/SF-IM catalyst were lower than that of Ni/SP-IM catalyst, which implied that methane steam reforming (Eq.(3)) and water gas shift reaction (Eq.(4)) activity on Ni/SF-IM catalyst were favorable. Moreover, the C_2H_6 selectivity and C_2H_4 selectivity over Ni/SP-IM catalyst were higher than Ni/SF-IM catalyst which indicated that Ni/SP-IM catalyst was easy to formation of coke as reported in literature [42, 51, 62]. In addition, the amount of acetaldehyde was higher detected over the Ni/SP-IM catalyst than Ni/SF-IM catalyst, suggesting a higher C-C bond cleavage reactivity of the Ni/SF-IM catalyst.

$$C_2H_5OH + 3H_2O \longrightarrow 2CO_2 + 6H_2 \tag{1}$$

$$C_2H_5OH \longrightarrow H_2 + CO + CH_4 \tag{2}$$

$$CH_4 + 2H_2O \longrightarrow CO_2 + 4H_2 \tag{3}$$

$$CO + H_2O \longrightarrow H_2 + CO_2 \tag{4}$$
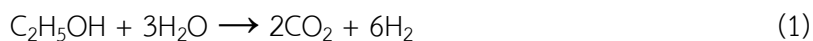
Kim et al. [55] pointed out that nanofiber catalyst revealed superior catalytic activity in WGS reaction compared to conventional bulk catalyst. His results were in agreement with Tang et al. [63] The observed results from both authors consisted with our expectation that WGS reaction might be the main reason for high selectivity to H_2 and CO_2 over the fiber catalyst because metal dispersed on the surface of fiber catalyst provided these active sites easily accessible to reactants.

4.2.2. Effect of temperature

Figure 21 Effect of reaction temperature on ethanol conversion and products distribution over Ni/SP-IM and Ni/SF-IM catalysts within 6 h time on stream. Reaction conditions: S/E: 9, W/F: 18 $g_{catalyst} \cdot h/mol_{ethanol}$.

Figure 21 shows catalytic performance in ESR at the temperature range from 400°C to 700°C, 1.0 atm, 18 $g_{catalyst} \cdot h/mol_{ethanol}$ and ethanol/steam molar ratio of 9. Regarding all catalysts, the catalytic activity increased with the increase in temperature. At low temperature (400°C), ethanol conversion was obtained 77.0% and 82.0%

corresponding to Ni/SP-IM and Ni/SF-IM. The Ni/SP-IM indicated apparently 1.1% of acetaldehyde selectivity when comparing to 0.2% acetaldehyde selectivity of Ni/SF-IM. That was definitely implied that the Ni/SF-IM was higher C-C cleavage ability than that of Ni/SP-IM catalyst. Nevertheless, both catalysts had presented C_2H_4 and C_2H_6 selectivity at low temperature which had lower C-C cleavage ability than high temperature. Additionally, higher selectivity of CO and CH_4 indicated that all of catalysts were active for ethanol decomposition to CO, CH_4 and H_2. And in the same time, the CO_2 selectivity was mainly produced from CO in water gas shift reaction due to the fact that the CO_2 production was favored at low temperature.

At temperature above 500°C, ethanol conversion were higher than 90 % over both catalysts and the acetaldehyde intermediates reacted completely. The CO_2 selectivity and H_2 yield increased while the CH_4 selectivity decreased were appeared due to methane steam reforming. The water gas shift reaction also presented at 500°C. However, low quantities of CO_2 were produced, implying that the capacity of WGS reaction was relatively weak. Hydrogen yield, which was 55% obtained over Ni/SF-IM catalysts, above the hydrogen yield over that of Ni/SP-IM. The results revealed clearly that Ni/SF-IM catalyst exhibited better than Ni/SP-IM catalyst.

4.2.3. Effect of steam/ethanol

Figure 22 presents the effect of steam/ethanol (S/E) molar ratio on the ethanol conversion and product distribution. These effect were investigated in the range of S/E from 1 to 12 molar ratio at 600°C, 1.0 atm, and space time 18 g_{cata}·h/mol$_{ethanol}$. For all catalysts, ethanol conversion and H_2 yield were increased with increasing S/E molar ratio because the formation of surface hydroxyl groups that were active in reforming was favored. CO_2 selectivity as well as increased, whereas CO and CH_4 selectivity decreased because CH_4 reforming and WGS reaction were much favored and methanation reaction was disfavored. Monica et al. [51] explained that a higher amount of surface hydroxyl groups inhibited the transformation of intermediate methyl groups into CH_4 because they were reacted with the methyl groups to produce CO_2. Moreover, the results reveal that excess of water favored the ESR reaction over ethanol decomposition [50]. For comparison between Ni/SP-IM and Ni/SF-IM catalysts, it shown

that the reaction over Ni/SF-IM catalyst was faster arriving equilibrium than that reaction over Ni/SP-IM catalyst. For Ni/SP-IM, the ESR reaction was more likely to occur than ethanol hydration with increasing of S/E molar ratio implying that, the amount of coke deposition on the catalyst decreased. Also, ethanol dehydration was favored in Ni/SP-IM catalyst because the porous catalyst has long time diffusion of reactants as well as low capacity to break the C-C bond that could be promoted the formation of ethane [64]. Thus, the optimum S/E molar ratio in ethanol steam reforming at 600°C, 1.0 atm, and space time 18 $g_{cata}\cdot h/mol_{ethanol}$ was 9.

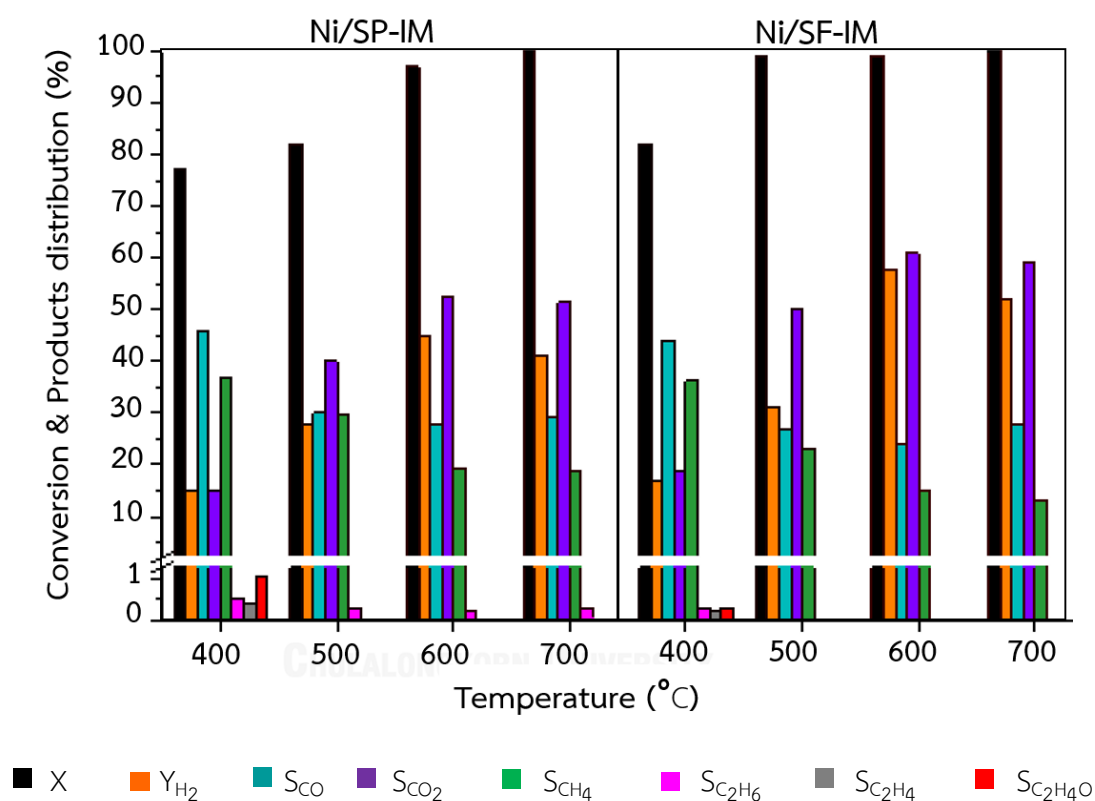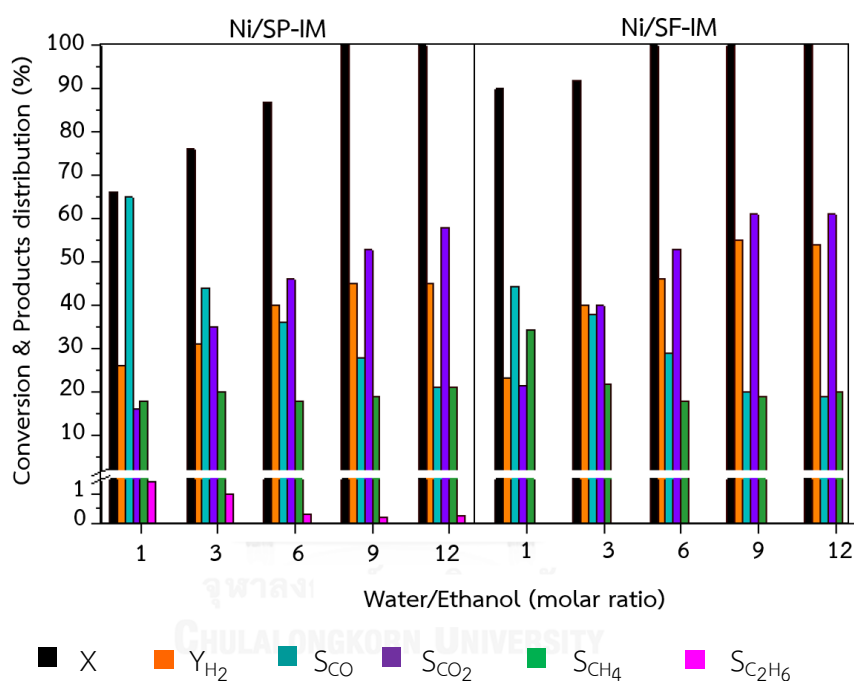*Figure 22* Effect of water/ethanol molar ratio in the feed on ethanol conversion and products distribution over Ni/SP-IM and Ni/SF-IM catalysts within 6 h time on stream. Reaction conditions: 600°C, W/F: 18 $g_{cata}\cdot h/mol_{ethanol}$.

4.2.4. Effect of space time

The effects of space time (W/F) on the ethanol conversion and products distribution were investigated in the range of space time from 12 to 36 $g_{cata}\cdot h/mol_{ethanol}$ at 600°C, 1.0 atm and ethanol/steam of 9. Figure 23 show catalytic performance in ESR with variation of space time. The ethanol conversion increased with the space time increasing from 12 to 18 $g_{catalyst}h/mol_{ethanol}$ and after that become constant. At low space time, the ethanol conversion was low because the velocity of ethanol and

steam through the active surface of catalyst was suddenly fast and then the contact time of ethanol and steam which contacted on the active site of catalyst was a short time. Thus, the thermodynamic equilibrium of the reaction was not completed. As space time increasing from 12 to 18 $g_{cata}\cdot h/mol_{ethanol}$, the H_2 yield increased from 38% to 55% with decreasing CH_4 selectivity from 23% to 15% over the Ni/SF-IM catalyst. This implies that methane steam reforming appeared dominantly. Whereas, the CH_4 selectivity over the Ni/SP-IM was constant which indicated that the MSR activity was lower activity than Ni/SF-IM catalyst due to effect of catalyst shape, resulting in lower ethanol conversion and H_2 yield. In contrast, the CO selectivity and CO_2 selectivity had a little convert. Moreover, ethanol dehydration was favored in Ni/SP-IM catalyst because the porous catalyst has long time diffusion of reactants as well as low capacity to break the C-C bond that could be promoted the formation of ethane [64]. Additionally, the ethanol conversion and products distribution had no obvious change with the space time increasing from 18 to 32 $g_{cata}\cdot h/mol_{ethanol}$. This result indicated that steam reforming and water gas shift reactions arriving equilibrium. Thus, the optimum space time value in ethanol steam reforming at 600°C, 1.0 atm, and ethanol/steam of 9 was 18 $g_{cata}\cdot h/mol_{ethanol}$.
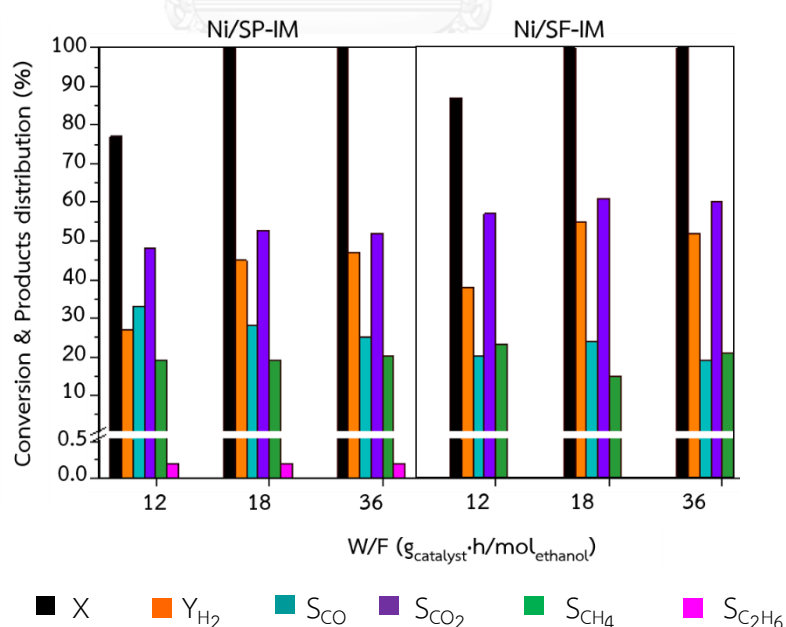
Figure 23 Effect of space time on ethanol conversion and products distribution over Ni/SP-IM and Ni/SF-IM catalysts within 6 h time on stream. Reaction conditions: 600°C, S/E: 9.

4.2.5. The steady state
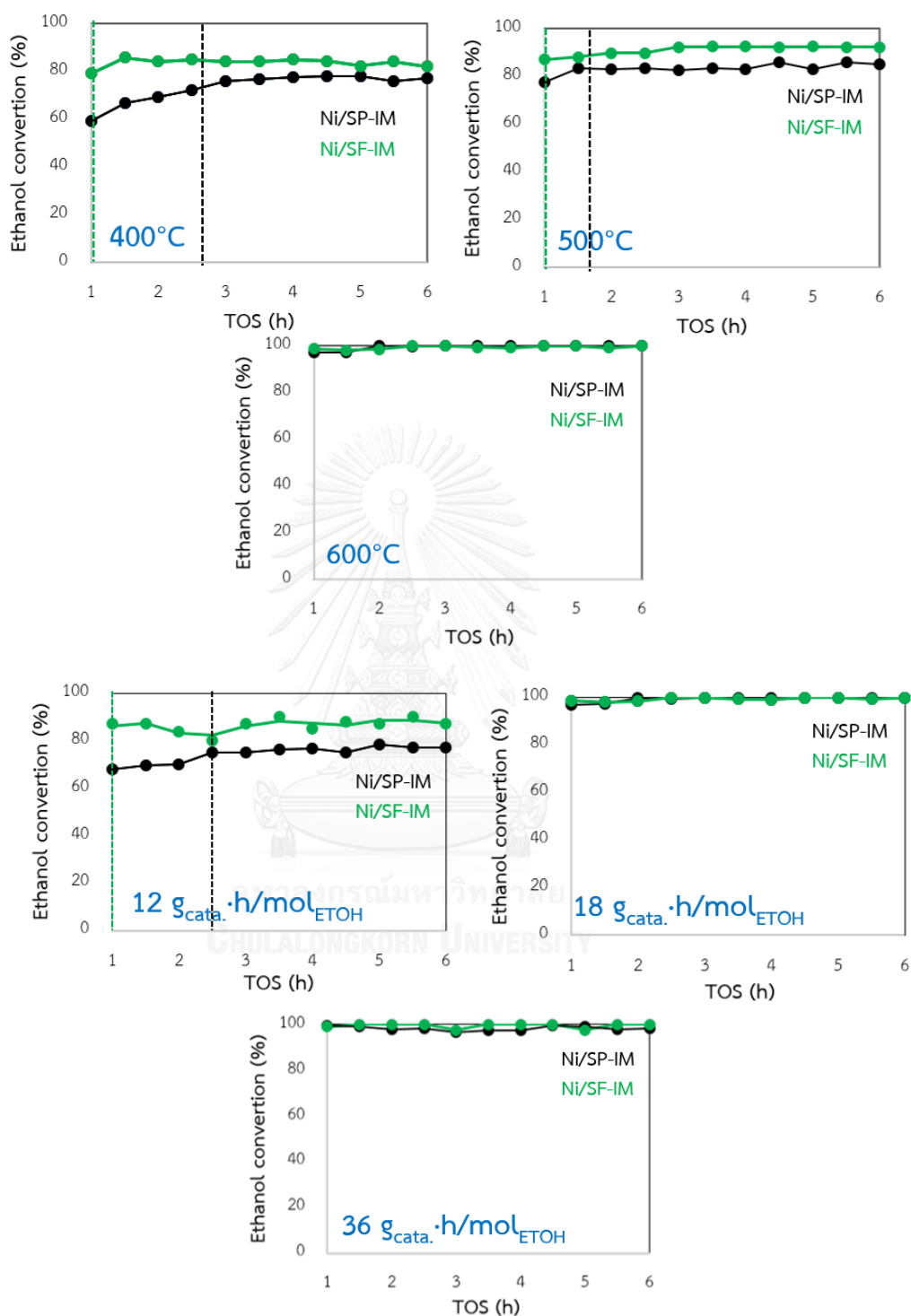
Figure 24 Ethanol conversion with time on stream over Ni/SP-IM and Ni/SF-SF catalysts.

Reaction conditions: (a) 400-600°C, S/E: 9:1, W/F: 18 $g_{cata.} \cdot h/mol_{ethanol}$

(b) 600°C, S/E: 9:1, W/F: 12, 18, and 36 $g_{cata.} \cdot h/mol_{ethanol}$.
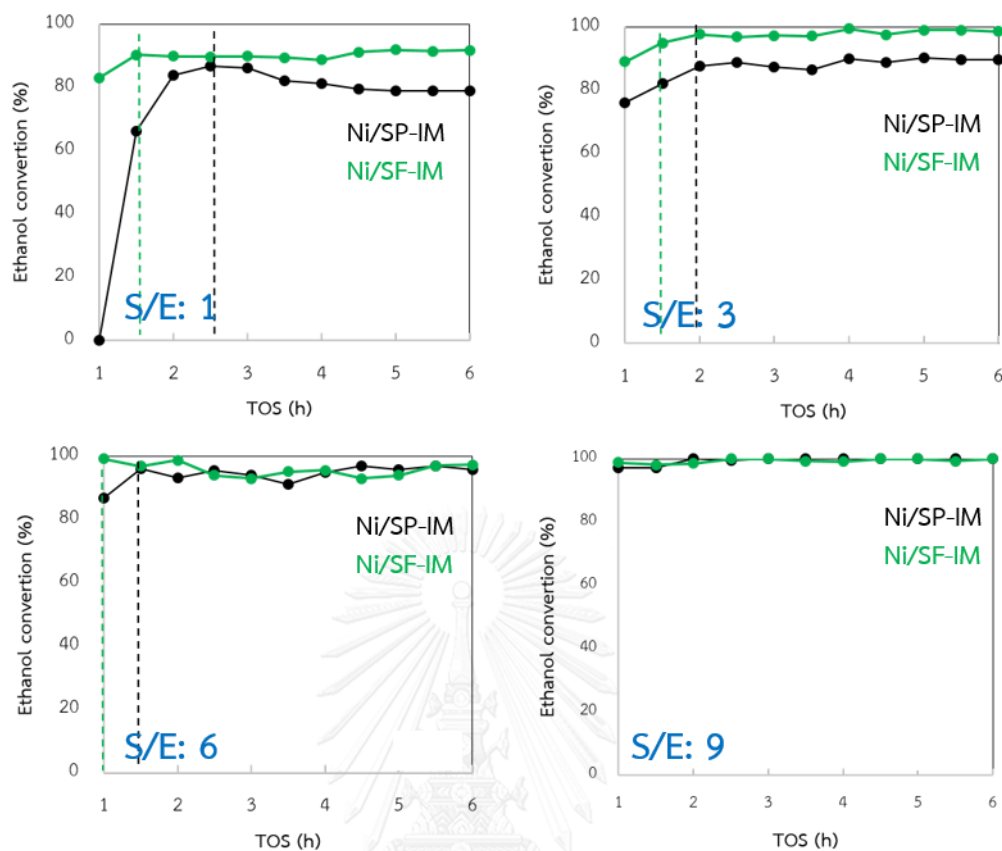
Figure 25 Ethanol conversion with time on stream over Ni/SP-IM and Ni/SF-SF catalysts
Reaction conditions: 400-600°C, W/F: 18 $g_{cata.}$·h/mol$_{ethanol}$, and S/E: 1, 3, 6, and 9.

The ethanol conversion as a function with time on stream of various parameter (i.e. reaction temperature, space time and water/ethanol molar ratio) was shown in Figure 24. For reaction temperature, over fiber catalyst, the ethanol conversion at 400°C was rapidly equilibrated within 1.5 h time on stream. Above 500°C, the conversion approach to the equilibrium at 1 h time on stream. Whereas, the conversion at 400°C of porous catalyst accessed to equilibrium at 3 h time on stream and into equilibrium at the beginning was 600°C. The trend of other parameters had gave the same results. Thus, the result reveals clearly that the conversion of fiber catalyst was faster approach to the equilibrium than that of porous catalyst leading to catalyst shape.

4.2.6. Effect of preparation methods over Ni/SF catalyst
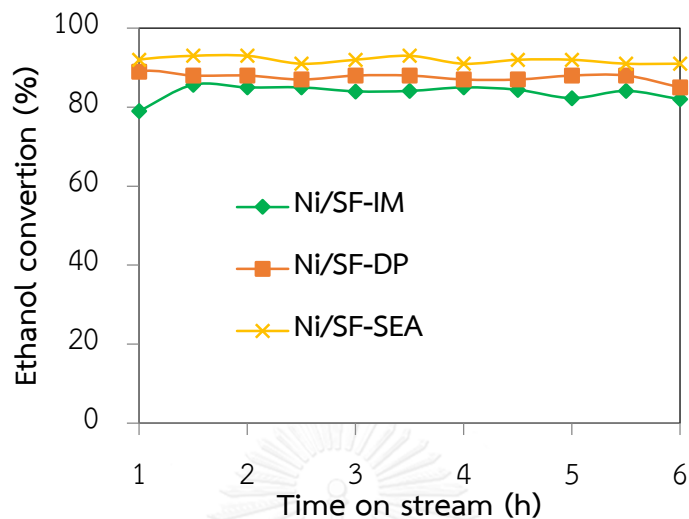
Figure 26 Ethanol conversion with time on stream over Ni/SF-IM, Ni/SF-DP and Ni/SF-SEA catalysts. Reaction conditions: 400℃, S/E: 9:1, W/F: 18 $g_{cata.}\cdot h/mol_{ethanol}$.
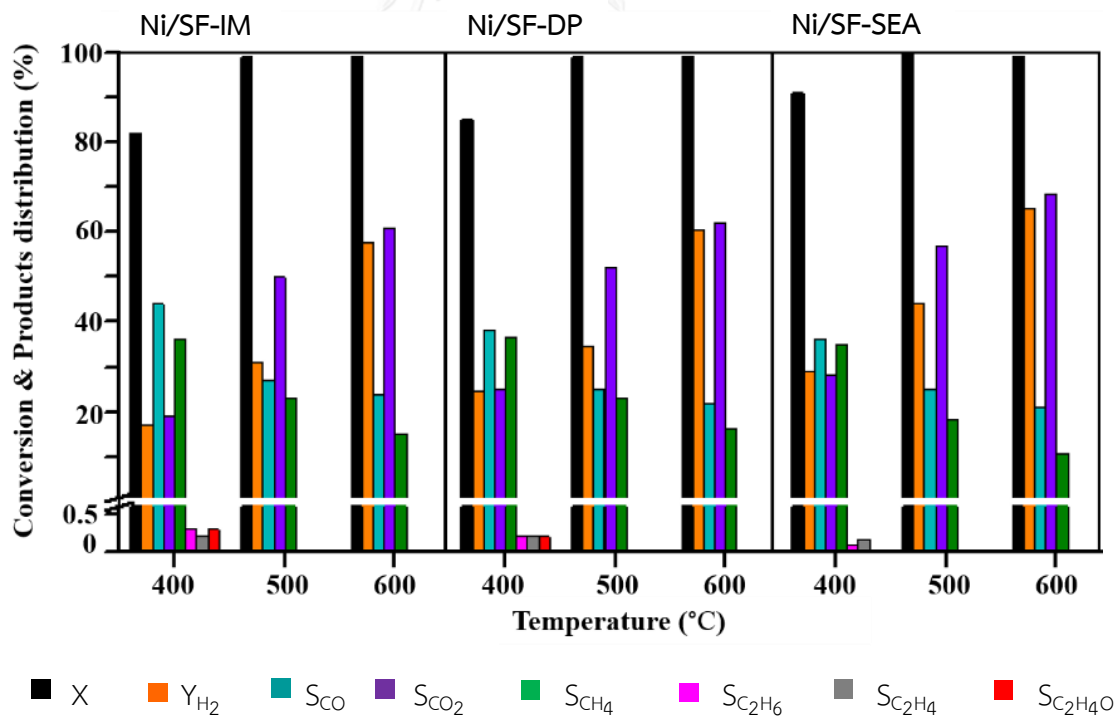
Figure 27 Effect of reaction temperature on ethanol conversion and products distribution over Ni/SF-IM, NiSF-DP and Ni/SF-SEA catalysts within 6 h time on stream. Reaction conditions: S/E: 9, W/F: 18 $g_{cata.}\cdot h/mol_{ethanol}$.

The ethanol conversions with time on stream at different fiber catalysts were shown in Figure 26. The effect of preparation methods on ethanol conversions revealed that ethanol conversions over Ni/SF-SEA (91.0%) was higher than that of Ni/SF-DP (85.5%) and Ni/SF-IM (82.0%) catalysts because the SEA method provided strong metal-support interaction, small particles size and well dispersion of nickel on the surface of support. While, IM method had large nickel particles due to the NiO particles can be easy to aggregate in the calcination step as seen in the XRD, H_2-TPR, SEM and TEM analysis (Figure 15, Figure 16, Figure 17, and Figure 18). The preparation method of Ni-based catalyst had been recommended that the small particle size of nickel and strong metal support interaction were enhanced the nickel catalyst activity in ESR [18]. The catalytic activity in ESR were ordered by Ni/SF-SEA >Ni/SF-DP >Ni/SF-IM.

Figure 27 show H_2 yield and selectivity of products, i.e. CO, CO_2, CH_4, C_2H_6, C_2H_4 and C_2H_4O in outlet steam with different catalysts at temperature range of 400-600°C with a water/ethanol molar ratio of 9 and 18 $g_{catalyst}$·h/$gmol_{EtOH}$ space time. Regarding all catalyst, The hydrogen yield increased as the temperature was increased due to enhanced steam reforming activity. At 400°C, The Ni/SF-IM and Ni/SF-DP catalysts indicated apparently 0.2% of acetaldehyde selectivity when comparing to 0% acetaldehyde selectivity of Ni/SF-SEA. That was definitely implied that the Ni/SF-SEA was higher C-C cleavage ability than that other catalysts. The acetaldehyde selectivity was low in the distribution of product gas because the faster and following dehydrogenation and decomposition of ethanol. Also, the presence of C_2H_6 and C_2H_4 gave at this temperature an indicating that the ethanol dehydration was favoured. As the temperature up to 500°C, no acetaldehyde (C_2H_4O) was observed over all catalyst. Also, the CO_2 selectivity and H_2 yield increased while the CO selectivity and CH_4 selectivity decreased were appeared due to water gas shift and methane steam reforming. Over the Ni/SF-SEA catalysts, the H_2 and CO_2 selectivity were quite high compared to other catalysts. When the temperature increased from 500°C to 600°C, The CO_2 selectivity and H_2 yield increased while the CH_4 selectivity decreased were appeared due to methane steam reforming. The water gas shift reaction also presented at this temperature. However, low quantities of CO_2 were produced, implying that the

capacity of WGS reaction was relatively weak. Hydrogen yield, which was higher than 60% obtained over Ni/SF-SEA and Ni/SF-DP catalysts. The order of hydrogen yield was as follows: Ni/SF-SEA> Ni/SF-DP> Ni/SF-IM. The result reveals clearly that Ni/SF-SEA catalyst exhibited better leading to small particles size and strong metal-support interaction.

4.2.7. Stability test
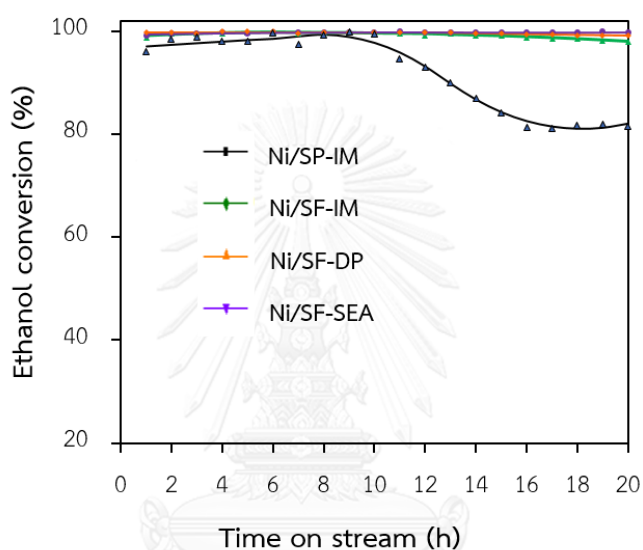
Figure 28 Stability test over different catalysts at 600°C, W/F: 18 $g_{cata.}\cdot h/mol_{ethanol}$, and S/E: 9:1.

To evaluate the endurance of Ni/SP-IM, Ni/SF-IM, Ni/SF-SEA and Ni/SF-DP catalysts, the stability test was performed at 600°C,1.0 atm, 18 $g_{cata.}\cdot h/mol_{ethanol}$ and ethanol/steam: 9 for 20 h. The results were showed in Figure 28. The ethanol conversion of Ni/SP-IM was completely at 100% within 10 h time on steam, and after 10 h, the ethanol conversion was decreased to 80% with rising selectivity of ethane. This implying that large amount of coke were deposited, that could be block catalyst pore. On the other hand, the catalyst deactivation didn't happen over nickel silica fiber catalysts. The ethanol conversion showed 100 % with constant throughout within 20 h. This indicating that silica fiber catalysts could be proven the pore blocked from coke. It was known that the catalyst structure had influence on catalytic performance.

Bobadilla et al. [65] studied the effect of the shape of Ni on glycerol steam reforming. They found that the catalyst morphology had a strong influence on the reforming process. Coking reaction over catalyst, having pore, was grown in the in the interparticle space blocking, resulting in pore blocking and loss of Ni active sites. In this work, the fiber catalyst had no pore. As for this results, it was implied that the fiber catalyst had better catalytic stability.

4.3. Characterization of spent catalyst

4.3.1. TGA-DTA
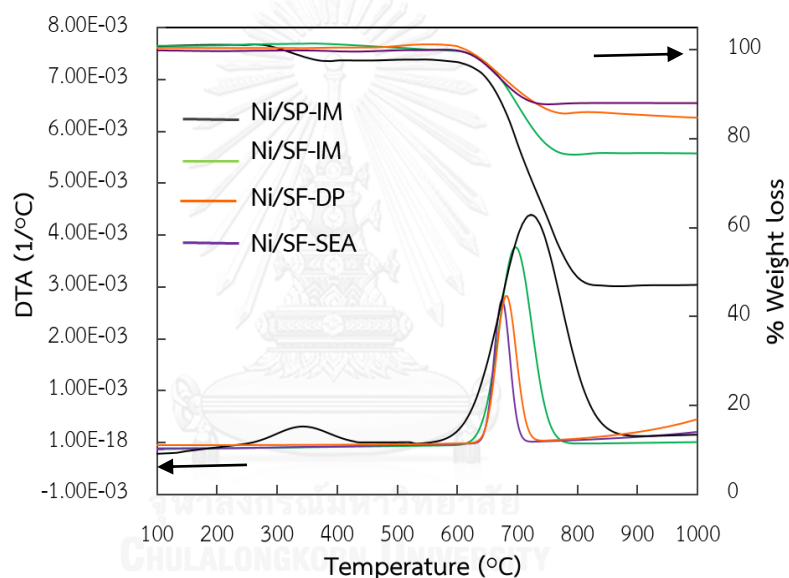
Figure 29 TGA-DTA curves of spent catalysts after 20 h stability test.

Figure 29 shows the TGA-DTA results of the spent catalysts after 20 h stability test. The TGA-DTA curves of all catalysts showed weight loss and the exothermic peaks should be attributed to the combustion of coke deposited. As could be seen, for Ni/SP-IM was two presented weight loss step in the temperature of 300°C-450°C and 600°C-850°C, indicating of two type of combustion of coke i.e., amorphous carbon and carbon nanofibers respectively. The type of coke with amorphous carbon was the main effect for the catalyst deactivation by blocking the active site [66, 67]. In comparison, the Ni/SF-IM, Ni/SF-SEA and Ni/SF-DP were presented only weight loss in the temperature range of 500°C-700°C attributed to the carbon nanofiber. Kim et al. [68]

explained that the mass loss in the temperature range of 610°C-720°C was assigned to the primary coke and the mass loss appeared higher 700°C was the combustion of graphite carbon. For Ni/SF-SEA and Ni/DF-DP catalysts mass loss above 700°C were not appeared, implying that the carbon nanofiber that was form in primary coke. The amount of carbon deposition on catalyst determined by TGA increased in the order: Ni/SP-IM > Ni/SF-IM >Ni/SF-DP > Ni/SF-SEA as shown in Table 3. This suggested that Ni/SF-DP and Ni/SF-SEA catalysts had the better character of coke resistance, which could be leading to small particles size and strong metal-support interaction. These results were agreement with TEM result. In addition, Kong et al. [69] investigated toluene reforming by various nickel catalysts, and reported that a larger amount of coke deposition was obtained for the catalyst (Ni/ZrO$_2$ and Ni/SiO$_2$) with large Ni particle size (23.6, and 26.8 nm, respectively) compared with the Ni/Al$_2$O$_3$ and Ni/MgO catalysts with Ni particle sizes less than 10 nm. Small Ni particle size was also reported to prohibit coke formation on a Ni-based catalyst during steam methane reforming [21, 70].

Table 3 Textural properties of the spent nickel catalysts

Samples	Weight loss (%)
Ni/SP-IM	51.9
Ni/SF-IM	30.4
Ni/SF-DP	15.9
Ni/SF-SEA	12.0

4.3.2. Transition electron microscopy (TEM)

Figure 30 shows TEM micrographs of spent catalysts after stability test. Over spent catalysts after 20 h stability test, some CNTs and CNFs shape observed on the catalysts surface, which indicated the locating of carbon deposition. For Ni/SP-IM, the deposits of amorphous carbon was observed, which seem to cover the catalyst particle

blocking the reactants access to the active metal and leading to the deactivation of catalyst. On the other hand, the amorphous carbon was not observed on Ni/SF catalysts. Moreover, the Ni dispersion and the mean metal particle size for all catalysts was compared in Figure 30. The metal active particle size of both catalyst i.e., Ni/SP-IM (Figure 30a) and Ni/SF-IM (Figure 30b) had large Ni particle due to low interaction of nickel with the support causing the ease of sintering and deactivation of catalyst. In contrast, nickel particles were smaller and well- dispersed on Ni/SF-SEA and Ni/SF-DP catalysts. This indicated that, the catalysts had strong metal–support interaction between Ni and support lead to resistance to sintering. The particle size of Ni calculated from TEM images were in the range of 8-35 nm as presented in Table 4. The mean particle size of NiO were ordered by Ni/SF-SEA <Ni/SF-DP <Ni/SP-IM <Ni/SF-IM, which was agreement with the XRD result (Figure 31).
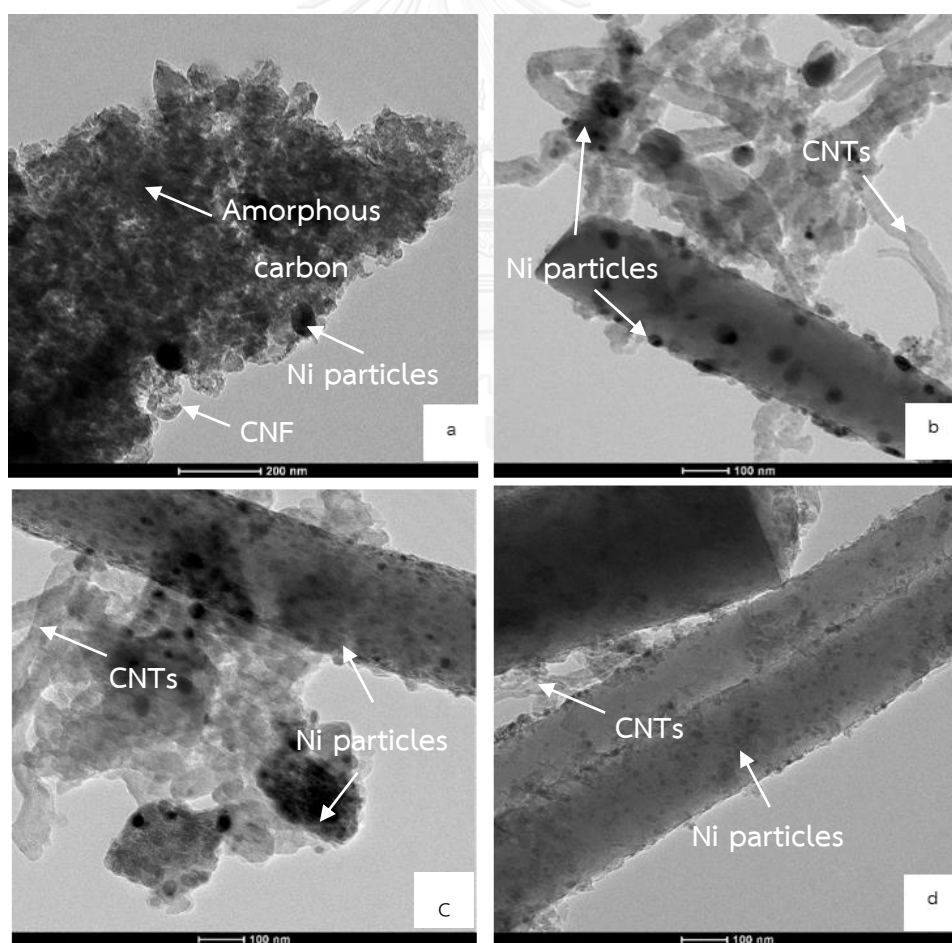
Figure 30 TEM micrographs of the spent catalysts after 20 h stability test: (a) Ni/SP-IM, (b) Ni/SF-IM, (c) Ni/SF-DP and (d) Ni/SF-SEA.

4.3.3. X-ray diffraction (XRD)

The XRD pattern of the spent nickel catalysts were presented in Figure 31.
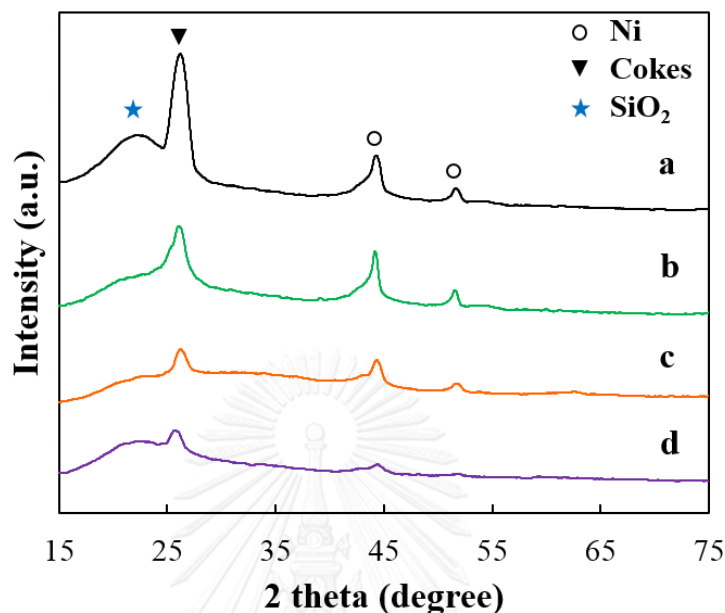
Figure 31 X-ray diffraction patterns after 20 h stability test of spent nickel catalysts: (a) Ni/SP-IM, (b) Ni/SF-IM, (c) Ni/SF-DP and (d) Ni/SF-SEA

.

In order to investigate the structure and Ni particle size of the spent catalysts, the XRD patterns of the spent catalysts after 20 h stability test were detected. The XRD patterns were presented in figure 16. The Ni phase showed peaks at 2 theta of 44.5° and 51.9° [21, 70]. A broad peak around 22° and 23 were referred to amorphous silica and coke respectively. The size of Ni particles calculated by the Scherrer's equation from the Ni (2 0 0) crystal plane was 37 nm for Ni/SP-IM, 36 nm for Ni/SF-IM, 8 nm for Ni/SF-SEA, and 16 nm for Ni/SF-DP. The particle size of spent catalysts prepared by impregnation method was large compared the particle size of fresh catalyst as a result from the sintering of the Ni particles. This was another main cause for the deactivation of catalyst during ethanol steam reforming. These results shown that SEA method had smaller Ni crystallite size than other methods after reaction. It was found that the catalyst prepared by impregnation method showed the weak metal-support interaction while the catalyst prepared by SEA and DP methods showed

the strong metal-support interaction, implying that the catalyst prepared by SEA and DP methods have stronger resistance to sintering and deactivation of catalyst.

Table 4 Textural properties of the spent nickel catalysts.

Samples	Ni content [a] (%)	Crystal size of fresh NiO XRD (nm)[b]	Crystal size of spent Ni^0	
			XRD (nm)[b]	TEM (nm)[c]
Ni/SP-IM	10.6	15	37	35
Ni/SF-IM	11.9	22	36	34
Ni/SF-SEA	10.6	7	8	8
Ni/SF-DP	11.0	14	16	17

[a] Ni content was analyzed by the EDX technique.

[b] The crystallite size of Ni^0 was calculate by the Scherrer's equation.

[c] The crystallite size of Ni^0 was calculate by TEM images.
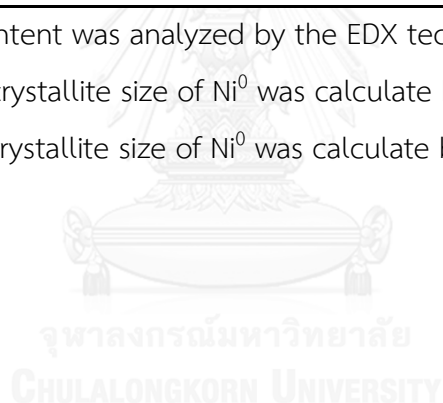
CHAPTER V

CONCLUSION

5.1. Conclusion

1. As a type of support shape of Ni-based catalysts prepared by impregnation method. The fiber catalyst (Ni/SF-IM) was more reducible than porous catalyst (Ni/SP-IM) because the Ni/SF-IM catalyst exhibited bigger particle size of NiO than Ni/SP-IM catalyst. For the catalytic performance in ethanol steam reforming, the ethanol conversion over porous catalyst was slightly lower than that of fiber catalyst because the porous catalyst had limit diffusion of reactants and products, resulting in the decrease of catalyst performance. Moreover, Ni/SP-IM catalyst had higher coke formation than Ni/SF-IM catalyst. TEM result was shown that carbon formation could block active Ni, resulting in low catalytic performance.

2. The catalytic activity increased with the increase in temperature. At low temperature (400°C), the Ni/SF-IM was higher C-C cleavage ability than that of Ni/SP-IM catalyst. Moreover, both catalysts had presented C_2H_4O selectivity at low temperature which had lower C-C cleavage ability than that high temperature. The maximum conversion was obtained in the temperature range of 500-600°C.

3. The ethanol conversion increased with increase steam/ethanol molar ratio because the formation of surface hydroxyl groups that were active in reforming was favored. Moreover, the addition of excess water favored the ESR reaction over ethanol decomposition. The maximum H_2 yield was obtained at H_2O/ETOH molar ratio of 9

4. The result was found that the effect of space time played an important role in ethanol steam reforming. The ethanol conversion increased with the space time increasing. At low space time, ethanol conversion decreased due to the velocity of ethanol and steam through the active surface of catalyst was suddenly fast and then the contact time of ethanol and steam which contacted on the active site of catalyst was a short time. Thus, the thermodynamic equilibrium of the reaction was not completed. Ethanol conversion over fiber catalyst was 99.9% at 18 g_{cata}·h/mol$_{ethanol}$ of space time.

5. The preparation method had a strong affect on catalytic performance of Ni/SF catalysts used in the ethanol steam reforming. The Ni/SF catalyst prepared by strong electrostatic adsorption method was smaller NiO particle size and stronger metal–support interaction than deposition precipitation and impregnation methods. The NiO particle size was 20, 14, and 7 nm for Ni/SF-IM, Ni/SF-DP and Ni/SF-SEA respectively. The catalyst with different size of NiO particle exhibited different catalytic activity. The strong metal–support interaction of catalyst enhanced the dispersion and surface area of nickel catalyst, resulting in high catalytic performance in ethanol steam reforming. The increase in both ethanol conversion and hydrogen yield were order by: Ni/SF-SEA >Ni/SF-DP >Ni/SF-IM. The Ni/SF-SEA catalyst exhibited the best catalytic activity in ethanol steam reforming which gave a high hydrogen yield of 65% and total ethanol conversion.

5.2. Recommendation

From the results of reaction temperature, it could be seen that the activity over all of nickel catalysts was complicated at different temperature and which could be ascribed to the effect of nickel metal and silica support. At low temperature of 400°C, the catalysts presented low ethanol conversion and hydrogen yield as well as the appearance of ethane, ethene, and acetaldehyde which implied that Ni catalyst had weaker ability of C-C bone cleavage at low temperature. Thus, to improve the ability of Ni catalyst at low temperature, the addition of promoters (such as lanthanum) or basic additive that favour water adsorption and coke gasification lead to enhanced the catalytic activity. Previous research explained that, lanthanum could promote dehydrogenation of ethanol and hinder ethanol dehydration bring to enhance the activity of hydrogen production on Ni catalyst at low temperature.

REFERENCES

1.   Dou, B., et al., *Hydrogen production from catalytic steam reforming of biodiesel byproduct glycerol: Issues and challenges.* Renewable and Sustainable Energy Reviews, 2014. **30**: p. 950-960.

2.   Lulianelli, A., et al., *Methanol steam reforming for hydrogen generation via conventional and membrane reactors: A review.* Renewable and Sustainable Energy Reviews, 2014. **29**: p. 355-368.

3.   Bilal, M. and S.D. Jackson, *Ethanol steam reforming over Rh and Pt catalysts: effect of temperature and catalyst deactivation.* Catalysis Science & Technology, 2013. **3**: p. 754-766.

4.   Karima, A.M., et al., *A comparative study between Co and Rh for steam reforming of ethanol.* Applied Catalysis B: Environmental, 2010. **96** p. 441–448.

5.   Freni, S., et al., *Steam reforming of ethanol on Ni/MgO catalysts: H_2 production for MCFC.* Journal of Power Sources 2002. **108**: p. 53-57.

6.   Choong, C.K.S., et al., *Effect of calcium addition on catalytic ethanol steam reforming of Ni/Al$_2$O$_3$: II. Acidity/basicity, water adsorption and catalytic activity.* Applied Catalysis A: General 2011. **407**: p. 155-162.

7.   Han, S.J., et al., *Hydrogen production by steam reforming of ethanol over mesoporous NieAl$_2$O$_3$-ZrO$_2$ xerogel catalysts: Effect of Zr/Al molar ratio.* international journal of hydrogen energy 2013. **38**: p. 1376-1383.

8.   Vizcaı́no, A.J., et al., *Hydrogen production by steam reforming of ethanol using Ni catalysts based on ternary mixed oxides prepared by coprecipitation.* International Journal of Hydrogen Energy 2012. **37**: p. 1985-1992.

9.   Silva, A.M.d., et al., *The effect of support reducibility on the stability of Co/CeO$_2$ for the oxidative steam reforming of ethanol.* Catalysis Today 2011. **164**: p. 234–239

10.   Valant, A.L., et al., *Preparation and characterization of bimetallic Rh-Ni/Y$_2$O$_3$-Al$_2$O$_3$ for hydrogen production by raw bioethanol steam reforming: influence*

of the addition of nickel on the catalyst performances and stability. Applied Catalysis B: Environmental, 2010. **97**: p. 72-81.

11. Wang, F., et al., *Hydrogen production from ethanol steam reforming over Ir/CeO$_2$ catalysts: Enhanced stability by PrO$_x$ promotion.* International Journal of Hydrogen Energy 2011. **36**: p. 13566-13574.

12. Siang, J.Y., et al., *Hydrogen production from steam reforming of ethanol using a ceria-supported iridium catalyst: Effect of different ceria supports.* International Journal of Hydrogen Energy 2010. **35**: p. 3456-3462.

13. Deng, X., et al., *Steam reforming of ethanol for hydrogen production over NiO/ZnO/ZrO$_2$ catalysts.* International Journal of Hydrogen Energy 2008. **33**: p. 1008-1013.

14. Zhu, J., et al., *The promoting effect of La, Mg, Co and Zn on the activity and stability of Ni/SiO$_2$ catalyst for CO$_2$ reforming of methane.* International Journal of Hydrogen Energy, 2011. **36**: p. 7094-7104.

15. Contreras, J.L., et al., *Catalysts for H$_2$ production using the ethanol steam reforming (a review).* International Journal of Hydrogen Energy 2014. **39**: p. 18835-18853.

16. Bang, Y., et al., *Hydrogen production by steam reforming of liquefied natural gas (LNG) over mesoporous Ni/Al$_2$O$_3$ catalyst prepared by an EDTA-assisted impregnation method.* Applied Catalysis B: Environmental 2016. **180**: p. 179-188.

17. Bertone, M.E., et al., *Highly selective conversion of maleic anhydride to butyrolactone over Ni-supported catalysts prepared by precipitation–deposition method.* Applied Catalysis A: General 2015. **503**: p. 135-146.

18. Jiao, L. and J.R. Regalbuto, *The synthesis of highly dispersed noble and base metals on silica via strong electrostatic adsorption: I. Amorphous silica.* Journal of Catalysis 2008. **260**: p. 329-341.

19. Hou, T., et al., *Hydrogen production from ethanol reforming: Catalysts and reaction mechanism.* Renewable and Sustainable Energy Reviews 2015. **44**: p. 132-148.

20. Vicente, J., et al., *Reaction pathway for ethanol steam reforming on a Ni/SiO$_2$ catalyst including coke formation.* International Journal of Hydrogen Energy 2014. **39**: p. 18820-18834.

21. Zhang, C., et al., *Synthesis of stable Ni-CeO$_2$ catalysts via ball-milling for ethanol steam reforming.* Catalysis Today 2014. **233**: p. 53-60.

22. Rabenstein, G. and V. Hacker, *Hydrogen for fuel cells from ethanol by steam-reforming, partial-oxidation and combined auto-thermal reforming: A thermodynamic analysis.* Journal of Power Sources, 2008. **185**(2): p. 1293-1304.

23. Aupreetre, F., et al., *Bio-ethanol catalytic steam reforming over supported metal catalysts.* Catalysis Communications 2002. **3**: p. 263-267.

24. Wu, X. and S. Kawi, *Steam reforming of ethanol to H$_2$ over Rh/Y$_2$O$_3$: crucial roles of Y$_2$O$_3$ oxidizing ability, space velocity, and H$_2$/C†.* Energy & Environmental Science, 2010. **3**: p. 334–342.

25. Roh, H.S., et al., *Low Temperature and H$_2$ Selective Catalysts for Ethanol Steam Reforming.* Catalysis Letters, 2006. **108**(1-2): p. 15-19.

26. Scott, M.S., et al., *Structural Analysis of Rh–Pd/CeO$_2$ Catalysts Under Reductive Conditions: An X-ray Investigation.* Topics in Catalysis, 2014. **58**(2-3): p. 123-133.

27. Ma, H., et al., *Efficient hydrogen production from ethanol steam reforming over La-modified ordered mesoporous Ni-based catalysts.* Applied Catalysis B: Environmental, 2016. **181**: p. 321-331.

28. Ma, H., *Efficient hydrogen production from ethanol steam reforming over La-modified ordered mesoporous Ni-based catalysts Applied Catalysis B: Environmental* Applied Catalysis B: Environmental, 2016. **181**: p. 321-331.

29. Regmi, M., et al., *Ethanol reactions over RuePt/CeO$_2$ catalysts.* 2011: ACS National Meeting Book

30. Chiou, J.Y.Z., et al., *Pathways of ethanol steam reforming over ceria-supported catalysts.* International Journal of Hydrogen Energy, 2012. **37**(18): p. 13667-13673.

31. He, Z., et al., *Effect of the transition metal oxide supports on hydrogen production from bio-ethanol reforming.* Catalysis Today, 2012. **194**(1): p. 2-8.

32. Zhang, B., et al., *Steam reforming of bio-ethanol for the production of hydrogen over ceria-supported Co, Ir and Ni catalysts.* Catalysis Communications, 2006. **7**(6): p. 367-372.

33. Palma, V., et al., *Hydrogen production through catalytic low-temperature bio-ethanol steam reforming.* Clean Technologies and Environmental Policy, 2012. **14**(5): p. 973-987.

34. Ciambelli, P., et al., *Low temperature catalytic steam reforming of ethanol. 1. The effect of the support on the activity and stability of Pt catalysts.* Applied Catalysis B: Environmental, 2010. **96**(1-2): p. 18-27.

35. Yang, Y., et al., *Production of hydrogen by steam reforming of ethanol over a Ni/ZnO catalyst.* International Journal of Hydrogen Energy, 2006. **31**(7): p. 877-882.

36. Fajardo, H.V., et al., *Influence of support on catalytic behavior of nickel catalysts in the steam reforming of ethanol for hydrogen production.* Environmental Chemistry Letters, 2008. **8**(1): p. 79-85.

37. Palma, V., et al., *Low temperature-ethanol steam reforming over Ni-based catalysts supported on CeO$_2$.* Journal of Power Technologies 2015. **95**: p. 54-66.

38. Duan, S. and S. Senkan, *Catalytic Conversion of Ethanol to Hydrogen Using Combinatorial Methods.* Industrial & Engineering Chemistry Research, 2005. **44**(16): p. 6381-6386.

39. Jo, S.W., et al., *Reasonable harmony of Ni and Mn in core@shell-structured NiMn@SiO$_2$ catalysts prepared for hydrogen production from ethanol steam reforming.* Chemical Engineering Journal, 2016. **288**: p. 858-868.

40. Bej, B., et al., *Production of hydrogen by steam reforming of ethanol over alumina supported nano-NiO/SiO$_2$ catalyst.* Catalysis Today, 2014. **237**: p. 80-88.

41. *ELECTROSPINNING APPARATUS.* [cited 2016 October, 20].

42. Yang, M., et al., *Ammonia-assisted synthesis towards a phyllosilicate-derived highly-dispersed and long-lived Ni/SiO$_2$catalyst.* Catal. Sci. Technol., 2015. **5**(12): p. 5095-5099.

43.   Li, G., L. Hu, and J.M. Hill, *Comparison of reducibility and stability of alumina-supported Ni catalysts prepared by impregnation and co-precipitation.* Applied Catalysis A: General, 2006. **301**(1): p. 16-24.

44.   Naeem, M.A., et al., *Hydrogen production from methane dry reforming over nickel-based nanocatalysts using surfactant-assisted or polyol method.* International Journal of Hydrogen Energy, 2014. **39**(30): p. 17009-17023.

45.   Burattin, P., M. Che, and C. Louis, *Metal Particle Size in Ni/SiO$_2$ Materials Prepared by Deposition-Precipitation: Influence of the Nature of the Ni(II) Phase and of Its Interaction with the Support.* J. Phys. Chem. B. **103**: p. 6171-6178.

46.   Munnik, P., et al., *Recent developments in the synthesis of supported catalysts.* Chem Rev, 2015. **115**(14): p. 6687-718.

47.   Wang, L., et al., *Effect of precipitants on Ni-CeO$_2$ catalysts prepared by a co-precipitation method for the reverse water-gas shift reaction.* Journal of Rare Earths, 2013. **31**(10): p. 969-974.

48.   Sun, S. and H. Zeng, *Size-Controlled Synthesis of Magnetite Nanoparticles.* Journal of the American Chemical Society, 2002. **124**(28): p. 8204-8205.

49.   Gayubo, A.G., et al., *Comparison of Ni and Co Catalysts for Ethanol Steam Reforming in a Fluidized Bed Reactor.* Catalysis Letters, 2014. **144**(7): p. 1134-1143.

50.   Frusteri, F., et al., *Steam and auto-thermal reforming of bio-ethanol over MgO and CeO$_2$ Ni supported catalysts.* International Journal of Hydrogen Energy, 2006. **31**(15): p. 2193-2199.

51.   Haryanto, A., et al., *Current Status of Hydrogen Production Techniques by Steam Reforming of Ethanol: A Review.* Energy & Fuels, 2005. **19**(5): p. 2098-2106.

52.   Lindo, M., et al., *Ethanol steam reforming on Ni/Al-SBA-15 catalysts: Effect of the aluminium content.* International Journal of Hydrogen Energy, 2010. **35**(11): p. 5895-5901.

53.   Klaigaew, K., et al., *Effect of preparation methods on activation of cobalt catalyst supported on silica fiber for Fischer–Tropsch synthesis.* Chemical Engineering Journal, 2015. **278**: p. 166-173.

54. Reubroycharoen, P., N. Tangkanaporn, and C. Chaiya, *Ni/SiO₂ fiber catalyst prepared by electrospinning technique for glycerol reforming to synthesis gas.* 2010. **175**: p. 689-693.

55. Kim, H., et al., *Preparation of Pt-loaded TiO₂ nanofibers by electrospinning and their application for WGS reactions.* Applied Catalysis A: General, 2009. **352**(1-2): p. 265-270.

56. Zhang, C., et al., *Hydrogen Production via Steam Reforming of Ethanol on Phyllosilicate-Derived Ni/SiO₂: Enhanced Metal–Support Interaction and Catalytic Stability.* ACS Sustainable Chemistry & Engineering, 2012: p. 161-173.

57. Donphai, W., et al., *Effect of Ni-CNTs/mesocellular silica composite catalysts on carbon dioxide reforming of methane.* Applied Catalysis A: General, 2014. **475**: p. 16-26.

58. Sietsma, J.R.A., J.D. Meeldijk, and A. Broersma, *Ordered Mesoporous Silica to Study the Preparation of Ni/SiO₂ ex Nitrate Catalysts: Impregnation, Drying, and Thermal Treatments.* Chem. Mater. , 2008. **20**: p. 2921–2931.

59. Liu, L., X. Ma, and J. Li, *Hydrogen production from ethanol steam reforming over Ni/SiO₂ catalysts: A comparative study of traditional preparation and microwave modification methods.* International Journal of Energy Research, 2014. **38**(7): p. 860-874.

60. Nares, R.n., et al., *Ni/Hβ-Zeolite Catalysts Prepared by Deposition-Precipitation.* J. Phys. Chem. B 2002. **106**: p. 13287-13293.

61. Kumar, A., et al., *Steam Reforming of Ethanol: Production of Renewable Hydrogen.* International Journal of Environmental Research and Development., 2014. **4**: p. 203-212.

62. Zeng, G., et al., *Kinetic and process study of ethanol steam reforming over Ni/Mg(Al)O catalysts: The initial steps.* Catalysis Today, 2016. **259**: p. 312-322.

63. Tang, H., et al., *Fabrication of Pt/CeO₂ nanofibers for use in water–gas shift reaction.* Materials Letters, 2012. **77**: p. 7-9.

64. Osorio-Vargas, P., et al., *Improved stability of Ni/Al₂O₃ catalysts by effect of promoters (La₂O₃, CeO₂) for ethanol steam-reforming reaction.* Catalysis Today, 2016. **259**: p. 27-38.

65.   Bobadilla, L.F., et al., *Glycerol steam reforming on bimetallic NiSn/CeO$_2$–MgO–Al$_2$O$_3$ catalysts: Influence of the support, reaction parameters and deactivation/regeneration processes.* Applied Catalysis A: General, 2015. **492**: p. 38-47.

66.   Osorio-Vargas, P., et al., *Improved ethanol steam reforming on Rh/Al$_2$O$_3$ catalysts doped with CeO$_2$ or/and La$_2$O$_3$: Influence in reaction pathways including coke formation.* Applied Catalysis A: General, 2015. **505**: p. 159-172.

67.   Montero, C., et al., *Monitoring Ni0 and coke evolution during the deactivation of a Ni/La$_2$O$_3$–αAl$_2$O$_3$ catalyst in ethanol steam reforming in a fluidized bed.* Journal of Catalysis, 2015. **331**: p. 181-192.

68.   Kim, D.H., et al., *Hydrogen production by steam reforming of ethanol over Ni-Sr-Al$_2$O$_3$-ZrO$_2$ aerogel catalyst.* Journal of Molecular Catalysis A: Chemical, 2016. **424**: p. 342-350.

69.   Kong, M., et al., *Influence of supports on catalytic behavior of nickel catalysts in carbon dioxide reforming of toluene as a model compound of tar from biomass gasification.* Bioresour Technol, 2011. **102**(2): p. 2004-8.

70.   Garbarino, G., et al., *A study of Ni/Al$_2$O$_3$ and Ni–La/Al$_2$O$_3$ catalysts for the steam reforming of ethanol and phenol.* Applied Catalysis B: Environmental, 2015. **174-175**: p. 21-34.

APPENDIX

Appendix A

Calculation

1. Calculation for preparation of silica fiber (SF) samples

Molar ratio of TEOS:EtOH:H_2O:HCl = 1:2:2:0.01

	MW (g/mol)	Density (g/cm³)
TEOS (purity 95%)	208.33	0.933
EtOH	46.07	0.789
H_2O	18.00	1.00
HCl	36.46	1.18
Silica	60.09	2.20

TEOS 1 mol = silica 1 mol

Basis of silica 7.5 g

Therefore,

mole of TEOS =7.5/60.09 =0.125g

weight of TEOS =(0.125x208.33x100)/95 =27.4g

volume of TEOS = 27.4/0.933 = 29.3g

At TEOS = 0.1248 mol

Thus TEOS:EtOH:H_2O:HCl = 0.125:0.249:0.249:1.2x10⁻³

Therefore,

volume of ETOH = (0.249x46.09)/0.789 = 14.56 ml

volume of H_2O = (0.249x18)/1 = 4.49 ml

volume of HCl = (1.2x10⁻³x36.46)/1.18 = 0.04 ml

2. Calculation for preparation of 10 wt% Ni loading

Ni precursor; $Ni(NO_3)_2\cdot 6H_2O$

Ni (MW = 58.69 g/mol)

$Ni(NO_3)_2\cdot 6H_2O$ (MW = 290.81 g/mol)

Basis 0.9 g of silica fiber

Ni = (10x0.9)/90 = 0.1g

Weight of $Ni(NO_3)_2\cdot 6H_2O$ = (0.1x290.81)/58.69 = 0.495g

3. Calculation of crystalline size from X-ray diffraction (XRD)

The nickel oxide (NiO) particle can be estimated based on Scherrer equation

$$d(NiO) = \frac{K\lambda}{\beta cos\theta}$$

Where $d(NiO)$ is the crystallite size of NiO (nm)

λ is the X-ray wavelength (CuKα = 0.154nm)

θ is the diffraction angel

K is a constant (usually K = 1)

β is the line broadening at half of the maximum intensity (in radian unit)

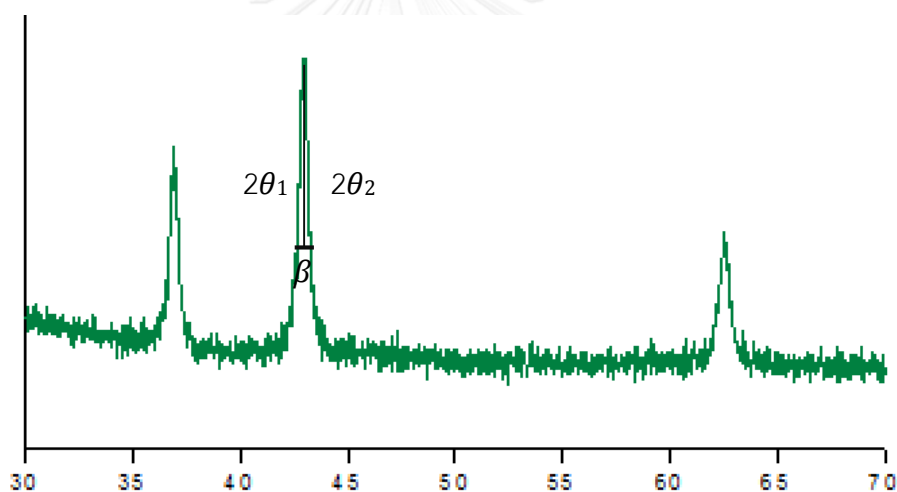The nickel particle size was calculated based on NiO particle size as equation following

Figure-A1 XRD pattern of Ni/SF-IM catalyst

Example: 10 wt.% Ni/SF-IM

$2\theta_1$ = 42.52°, $2\theta_2$ = 43.73°, θ = 1.21 = (3.14 x 1.21)/180° = 0.021 radian

β = (3.14 x 0.395°)/180° = 6.89 x 10^{-3} radian

$d(NiO)$ = (1 x 0.154)/(6.89 x 10^{-3} x cos(0.021)) = 22.35 nm

4. ESR reaction

$$X_{(ETOH)} = \frac{F_{in} - F_{out}}{F_{in}} \times 100 \qquad (1)$$

When F_{in} = molar flow rate of ethanol inlet

            F_{out} = molar flow rate of ethanol outlet

$$S_{(i)} = \frac{F_{C_i}}{F_{C_{out}}} \times 100 \qquad (2)$$

Where F_{C_i} = molar flow rate of the carbon containing species (i) in the products,

            including CO, CO_2, CH_4, C_2H_4, C_2H_6 and CH_3CHO

            $F_{C_{out}}$ = molar flow rate of C atom total in gas outlet

$$Y_{H_2} = \frac{F_{H_2}}{6\,F_{in}} \times 100 \qquad (3)$$

When F_{H_2} = molar flow rate of the hydrogen product

For example,

Reaction conditions: Water/Ethanol mole ratio 9:1, feed flow rate 0.04 mL/min and

flow rate of gas output = 48.37 mL/min at 6 h.

Catalyst = 0.1 g   V = 22.4 lit (STP) = 22400 ml (STP)

	Area Standard	Area Sample
H_2	10048	652456
CO	21013	70810
CO_2	18185	195535
CH_4	226929	485734

Therefore F_{H_2} = 652456/10048 = 64.9 %

                   = ((64.9/100) x 48.37x1000)/22400) = 1.4027 mmol/min

          F_{CO} = 70810/21013= 3.4 %

                   = ((3.4/100) x 48.37x1000)/22400) = 0.0728 mmol/min

          F_{CO_2} = 195535/18185= 10.75 %

                   = ((10.7/100) x 48.37x1000)/22400) = 0.2323 mmol/min

          F_{CH_4} = 485734/226929= 2.14 %

                   = ((2.14/100) x 48.37x1000)/22400) = 0.0462 mmol/min

          $F_{C_{out}}$ = (CO + CO_2 + CH_4)

                   = 0.0728 + 0.2323 + 0.0462 =0.3513 mmol/min

F_{in} = 0.3526 mmol/min

F_{out} = 0.0 mmol/min

Therefore

X_{ETOH} (%) = ((0.3526-0.0)/0.3526) x 100 = 100 %

H_2 yield (%) = ((1.4027/0.3526)/(6 x 100) = 66.3 %

CO selectivity (%) = (0.0728/0.3513) x 100 = 20.7 %

CO_2 selectivity (%) = (0.2323/0.3513) x 100 = 66.2%

CH_4 selectivity (%) = (0.0462/0.3513) x 100 = 13.1 %
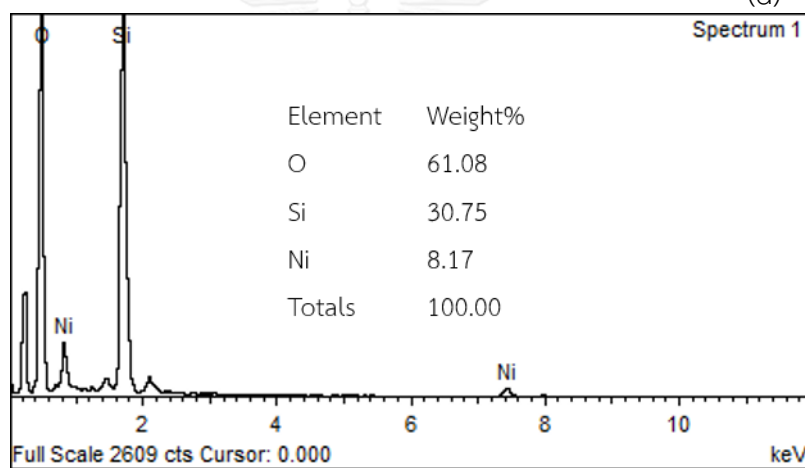
Appendix B

(a)

(b)
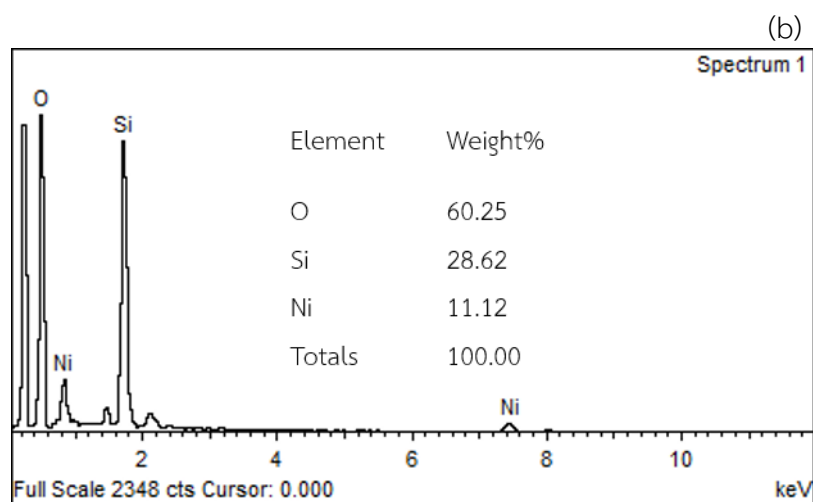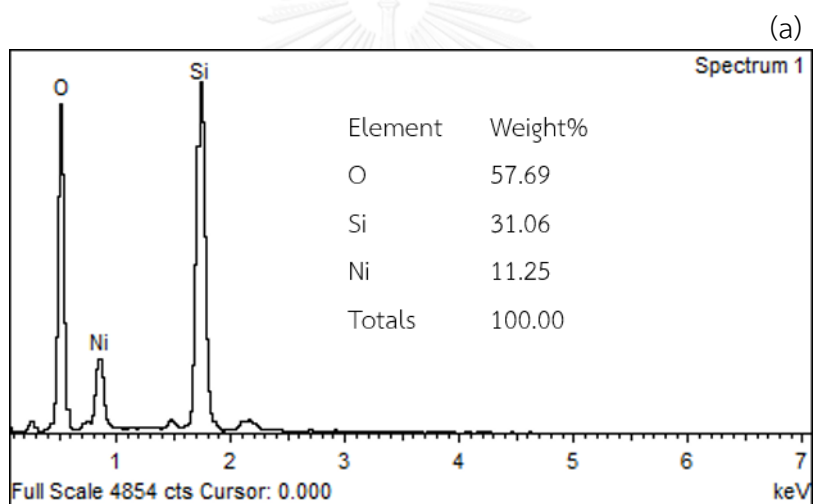
Figure-B1 EDX spectra of the calcinated catalyst: (a) Ni/SP-IM and (b) Ni/SF-IM.

(c)
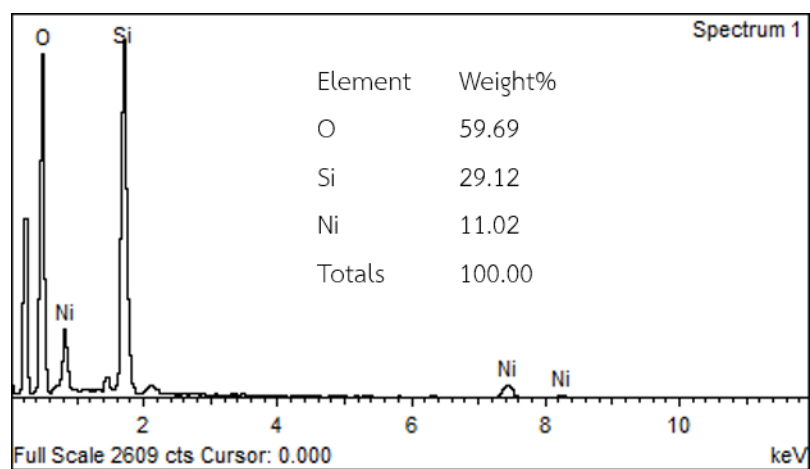
(d)

Figure-B2 EDX spectra of the calcinated catalyst: (c) Ni/SP-DP and (d) Ni/SF-SEA.

VITA

Miss Sareena Mhadmhan was born on February 1, 1991 in Phatthalung, Thailand. She graduated with Bachelor's degree of science, majoring in Chemistry, Faculty of Science, Prince of Songkla University in 2013. She has continued her study in program of Petrochemistry and Polymer Science, Faculty of Science, Chulalongkorn University, Bangkok, Thailand since 2014 and finished her study in 2016.

Poster presentation: Effects of Preparation Methods on the Activity of Ni/SiO2 Fiber Catalysts in Ethanol Steam Reforming. The 3rd Asian Conference on Biomass Science (ACBS2016), 1/19/2016, Niigata, Japan.